AD-A172 193 THE MEASUREMENT OF BOUNDARY LAYERS ON A COMPRESSOR BLADE IN CASCADE(U) PENNSYLVANIA STATE UNIV STATE COLLEGE APPLIED RESEARCH LAB S DEUTSCH ET AL. MAR 86 ARL/PSU/TR-8602 1/1

UNCLASSIFIED F/G 20/4 NL

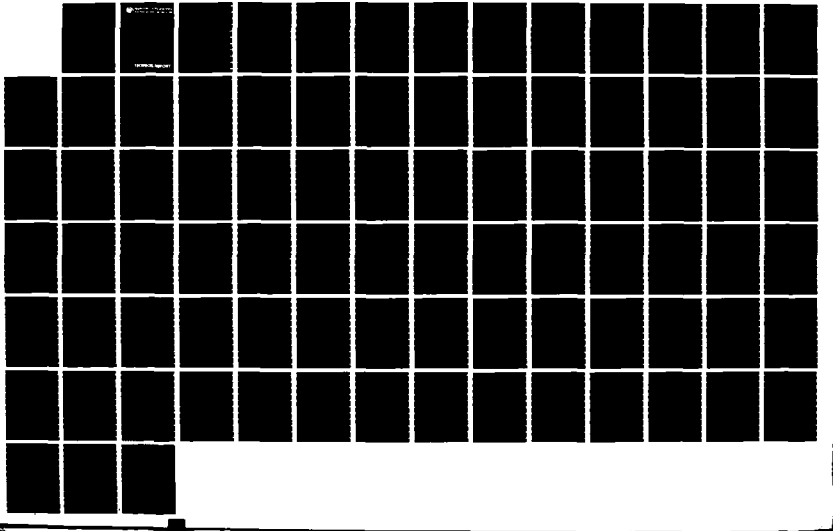

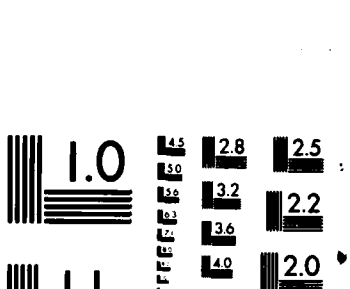

Applied Research Laboratory
The Pennsylvania State University

THE MEASUREMENT OF BOUNDARY LAYERS ON A COMPRES: BLADE IN CASCADE

by

Steve Deutsch and William C. Zierke

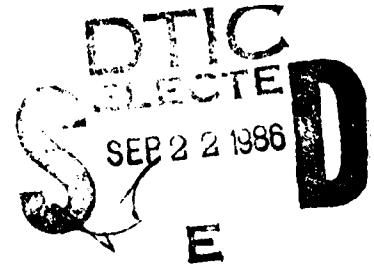

TECHNICAL REPORT

The Pennsylvania State University
Intercollege Research Programs and Facilities
APPLIED RESEARCH LABORATORY
P. O. Box 30
State College, PA 16804

THE MEASUREMENT OF BOUNDARY LAYERS ON A COMPRESSOR BLADE IN CASCADE

by

Steve Deutsch and William C. Zierke

Technical Report TR 86-02

March 1986

Supported by: NASA Lewis

L. R. Hettche, Director
Applied Research Laboratory

AD-A172 195

REPORT DOCUMENTATION PAGE

1a. REPORT SECURITY CLASSIFICATION Unclassified	1b. RESTRICTIVE MARKINGS
2a. SECURITY CLASSIFICATION AUTHORITY	3. DISTRIBUTION/AVAILABILITY OF REPORT
2b. DECLASSIFICATION/DOWNGRADING SCHEDULE	
4. PERFORMING ORGANIZATION REPORT NUMBER(S)	5. MONITORING ORGANIZATION REPORT NUMBER(S)
6a. NAME OF PERFORMING ORGANIZATION Applied Research Laboratory The Pennsylvania State Univ.	6b. OFFICE SYMBOL (If applicable) ARL
	7a. NAME OF MONITORING ORGANIZATION
6c. ADDRESS (City, State, and ZIP Code) P. O. Box 30 State College, PA 16804	7b. ADDRESS (City, State, and ZIP Code)
8a. NAME OF FUNDING/SPONSORING ORGANIZATION NASA	8b. OFFICE SYMBOL (If applicable)
	9. PROCUREMENT INSTRUMENT IDENTIFICATION NUMBER
8c. ADDRESS (City, State, and ZIP Code) Lewis Research Center Cleveland, OH 44135	10. SOURCE OF FUNDING NUMBERS PROGRAM ELEMENT NO. / PROJECT NO. / TASK NO. / WORK UNIT ACCESSION NO.

11. TITLE (Include Security Classification)
The Measurement of Boundary Layers on a Compressor Blade in Cascade

12. PERSONAL AUTHOR(S)
Steve Deutsch and William C. Zierke

13a. TYPE OF REPORT	13b. TIME COVERED	14. DATE OF REPORT (Year, Month, Day)	15. PAGE COUNT
Technical	FROM _____ TO _____	March 1986	78

16. SUPPLEMENTARY NOTATION

17. COSATI CODES			18. SUBJECT TERMS (Continue on reverse if necessary and identify by block number)
FIELD	GROUP	SUB-GROUP	compressor blade, mean velocity, experimental, cascade, turbulence, boundary layer

19. ABSTRACT (Continue on reverse if necessary and identify by block number)

Detailed measurements of the mean velocity and turbulence intensity were made using a one-component laser Doppler velocimeter in the boundary layer and near wake about a double circular arc, compressor blade in cascade. The measurements were made at a chord Reynolds number of 500,000. Boundary layer measurements on the pressure surface indicate a transition region over the last 40% of the chord. A small separation bubble near the leading edge of the suction surface results in an immediate transition from laminar to turbulent flow. The non-equilibrium turbulent boundary layers separate again near the trailing edge of the suction surface. Similarity of the outer region of the turbulent boundary layer ceases to exist in the separated region. Also, similarity does not hold in the near-wake region, a region which includes negative mean velocities because of the separation near the trailing edge of the suction surface.

20. DISTRIBUTION/AVAILABILITY OF ABSTRACT ☒ UNCLASSIFIED/UNLIMITED ☐ SAME AS RPT. ☐ DTIC USERS	21. ABSTRACT SECURITY CLASSIFICATION !
22a. NAME OF RESPONSIBLE INDIVIDUAL	22b. TELEPHONE (Include Area Code) / 22c. OFFICE SYMBOL

DD FORM 1473, 84 MAR — 83 APR edition may be used until exhausted. All other editions are obsolete.

Table of Contents

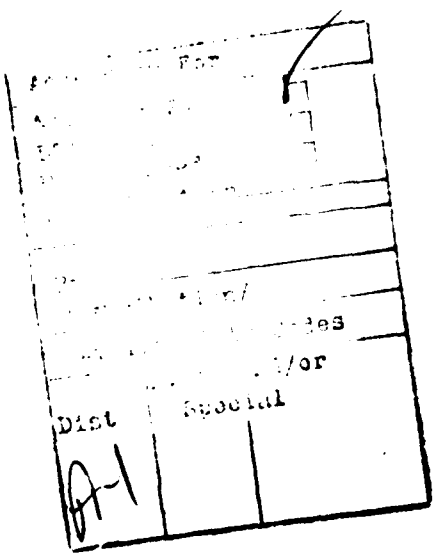

List of Figures

List of Figures (Cont'd)

ABSTRACT

Detailed measurements of the mean velocity and turbulence intensity were made using a one-component laser Doppler velocimeter in the boundary layer and near wake about a double circular arc, compressor blade in cascade. The measurements were made at a chord Reynolds number of 500,000. Boundary layer measurements on the pressure surface indicate a transition region over the last 40% of the chord. A small separation "bubble" near the leading edge of the suction surface results in an immediate transition from laminar to turbulent flow. The non-equilibrium turbulent boundary layers separate again near the trailing edge of the suction surface. Similarity of the outer region of the turbulent boundary layer ceases to exist in the separated region. Also, similarity does not hold in the near-wake region, a region which includes negative mean velocities because of the separation near the trailing edge of the suction surface.

INTRODUCTION

Over the past two decades, techniques for computing complex flows have become increasingly more sophisticated. Steger [1978], Thompson [1980], Rubin and Khosla [1981, 1982], Beam and Warming [1982], and Briley and McDonald [1984] have computed viscous flows at reasonable Reynolds numbers; Davis and Werle [1981] and Johnston and Sockol [1984] have studied viscid-inviscid interaction; and Edwards and Carter [1985] and Melnik and Brook [1985] have computed through separated regions. Further, all computations may now involve complex turbulence models, such as the models by Bradshaw, Ferriss, and Atwell [1967] and Launder, Reece, and Rodi [1975]. It is desirable that these techniques find their way into the design process. The design process of particular interest here is the turbomachinery design process. These numerical techniques are capable of very detailed predictions (for example, boundary layer profiles), but to be used *with confidence*, they should be tested against very detailed experimental data under typical flow conditions. As turbomachinery testing has generally been concerned with overall turbomachinery performance rather than with the details of the flow field, such data are lacking.

In order to provide some of the needed data, we used a one-component laser Doppler velocimeter (LDV) to measure the two-dimensional periodic flow field about a double circular arc, compressor blade in cascade. Eleven boundary layer profiles were taken on both the pressure and suction surfaces of the blade; two profiles were taken in the near wake. All measurements were made at a chord Reynolds number (Re_c) of 500,000 (±1%) and an incidence angle of 5 degrees (that is, the stagnation point is on the pressure surface). The turbulence intensity in the incident flow was 0.18%. With an incidence angle

of 5 degrees, the pressure surface exhibits a large region of laminar flow (up to roughly 60% chord); transition on the pressure surface appears to be incomplete. The suction surface profiles appear to separate both at the leading edge and again somewhat beyond midchord; the leading edge separation apparently reattaches by 2.6% chord. Using the terminology of Simpson, Chew, and Shivaprasad [1981], we found incipient detachment to occur at 60% chord on the suction surface and transitory detachment to occur at 83% chord. Inlet and outlet five-hole probe measurements and blade static-pressure measurements supplement the blade boundary layer profiles. Surface flow visualization, through sublimation, compliments the transition and separation region data. Before describing the experiment and its results, we will describe previous detailed measurements both in rotating systems and in cascades.

II. HISTORICAL BACKGROUND

Several researchers have attempted to measure boundary layers on turbomachine blades. Evans [1978] measured boundary layers at four chord (c) locations at midspan on the suction surface of a stator blade (c = 305.0 mm and Re_c = 500,000). The hot-wire measurements were made in an axial-flow compressor at three time-mean incidence angles on a row of stationary blades preceded by a row of rotating blades. The stator blades cut the wakes of the rotor blades and the rotor wake segments are subsequently transported through the stator passages. Since the wake segments involve low velocity fluid, the boundary layer is subject to a periodically varying freestream, and the blade is subject to a periodically varying incidence angle. Ensemble-averaged velocity profiles eliminate the random unsteadiness caused by turbulence. However, the periodic unsteadiness is preserved. The ensemble-averaged velocity profiles at 30% and 50% chord show that the boundary layers alternate between laminar and turbulent because of the unsteady flow. As a result, the

time-mean velocity profiles exhibited a larger boundary layer growth than was expected.

Anand and Lakshminarayana [1978] measured boundary layers on the rotor blades of a rocket pump inducer using a three-sensor hot-wire probe rotating with the blades. Because of imbalances in the radial pressure force and inertia forces in the blade boundary layer, outward radial velocities develop in a rotor blade boundary layer and inward radial velocities develop in a stator blade boundary layer. Anand and Lakshminarayana [1978] measured a significant outward radial component in the boundary layer velocity and found that this radial migration strongly influenced the chordwise velocity profiles.

Other experimenters have measured the boundary layers on rotor blades of axial-flow fans. Toyokura, Kurokawa, and Kimoto [1982] used rotating three-hole cobra probes to measure the three-dimensional boundary layers at six radial sections (c = 80.0 mm to 199.5 mm and Re_c = 300,000 to 500,000). The outward radial flow seemed to retard the predicted regions of transition and separation. Lakshminarayana, Govindan, and Hah [1982] used rotating miniature "x"-configuration hot-wire probes for boundary layer measurements at five radial locations (c = 152.4 mm and Re_c = 280,000 at midchord). Rotating miniature "x"-configuration hot-wire probes were also used by Pouagare, Galmes, and Lakshminarayana [1985] for numerous boundary layer measurements (c = 123.9 mm to 154.1 mm). In no case could the velocity profiles be very well resolved.

Walker [1982] made measurements similar to those of Evans [1978]. Walker [1982] used a hot wire in an axial-flow compressor to measure boundary layers on a stator (c = 76.0 mm and Re_c = 30,000 to 200,000) downstream of both a row of rotating blades and a row of inlet guide vanes. He tried to correct for

wall proximity using a method outlined by Wills [1962], but still had difficulties matching the law of the wall. Low Reynolds number, large adverse streamwise pressure gradients, and rapidly changing boundary conditions (due to the periodic unsteadiness) were given as reasons for the absence of a logarithmic region.

Hodson [1983] made hot-wire measurements in an axial-flow turbine at midspan on a rotor blade (c = 114.5 mm and Re_c = 315,000) downstream of a stator row. Once again, the periodic unsteadiness seemed to cause the boundary layer characteristics to vary between laminar and turbulent at some chordwise locations. Profile losses were larger than expected and this too was attributed to the unsteady flow.

Boundary layer measurements on turbomachine blades have yet to produce velocity profiles with enough detail and precision to compare with viscous computational codes. Therefore, our understanding of the physical nature of these complex, unsteady, three-dimensional boundary layers is far from complete. These flows are characterized by high turbulence levels, as well as by periodic unsteadiness caused by the interaction between stationary and rotating blade rows. "Blockage" effects exist because of the development of the end-wall boundary layers and the consequent contraction of the mainstream flow. The blade boundary layers are also affected by centrifugal and Coriolis forces associated with both the swirl and the blade rotation. The complex blade geometries and the complex flow field, including secondary flows, tip leakage, and trailing vorticity, make the analysis or measurement of turbomachine blade boundary layers very difficult.

Because of these difficulties, many researchers have sought a simple geometry which retains some of the physics of the flow in which to make their boundary layer measurements. A model that has proven effective in other areas

of turbomachinery is the periodic, two-dimensional row of airfoils, commonly referred to as a cascade. Properly realized, a cascade should eliminate all of the complexities of the turbomachine except blade curvature, secondary flow, and the effect of freestream turbulence.

The first attempt to measure boundary layers on cascade blades was made by Peterson [1958]. He used a three-hole cobra probe to measure blade boundary layers in a compressor cascade (c = 123.8 mm and Re_c = 300,000). Several boundary layers were measured on both the suction and pressure surfaces for three different incidence angles. In an attempt to better model an actual turbomachine, Peterson [1958] simulated the added diffusion caused by the radial distribution of axial velocity and the consequent streamline deviation. This added diffusion was created in the cascade by placing a perforated metal screen downstream of the blades. The measurements were not taken in the freestream, and therefore, the normal pressure gradient remains unknown. This lack of information leads to a problem in computing the edge velocity (which was probably inferred from the blade static-pressure distribution). The data are quite scattered, especially in the regions near separation, where the cobra probe fails. Peterson [1958] reported no significant differences between measurements with and without the added diffusion.

Pollard and Gostelow [1967] measured boundary layers on compressor cascade blades (c = 152.4 mm and Re_c = 200,000) with a Pitot tube to examine the effect of leading edge roughness. Three suction surface boundary layers and one pressure surface boundary layer were measured on both blades with a smooth leading edge and with a leading edge roughened with polythene spheres. With no roughness, laminar separation occurred before transition. It appears that separation of the turbulent boundary layers near the trailing edge would

be more likely to occur when leading edge roughness is present. These results agree with the Preston tube skin-friction measurements of Pollard and Gostelow [1967]. The detail and precision of the data are unknown since no actual data points are given.

Evans [1981] used compressor cascade blades (c = 304.8 mm and Re_c = 500,000) for boundary layer measurements taken with a hot-wire anemometer probe. A problem with this data is that the blade boundary layers were tripped with a wire at 10% chord. Evans [1971] argued that a turbulent boundary layer over most of the blade would better represent the high turbulence and unsteadiness levels usually encountered in a turbomachine. Instead, the artificially induced boundary layer development is rather misleading.

Problems of contamination, corrosion, erosion, and deposition have led to two investigations that dealt with the effects of surface roughness on cascade blade boundary layers. Bammert and Milsch [1972] measured blade boundary layers in a compressor cascade (c = 180.0 cm and Re_c = 430,000) with four different blade profiles to parametrically change the pitch, camber, and thickness of the blades. They used emery powder to develop the five roughness grades to be tested. A turbine cascade (c = 17.50 cm and Re_c = 560,000) was used for the blade boundary layer measurements of Bammert and Sandstede [1980] where four roughness grades were tested. Both investigations used a flattened Pitot tube which allowed measurements to be taken very close to the blade surface. Bammert and Sandstede [1980] used a hot-wire anemometer to confirm the measurements made with the flattened Pitot tube. The studies showed that increasing surface roughness led to increases in both momentum thickness and skin friction and a forward shift of the regions of transition and separation.

Meauzé [1979] used a transonic compressor cascade (c = 9.49 cm, Re_c = 1,660,000 for M_1 = 0.70, and Re_c = 2,120,000 for M_1 = 0.85) for blade boundary layer measurements. He used total-pressure probes to measure suction surface boundary layers for two inlet Mach numbers and four incidence angles. The flow recompression on the highly cambered blades results in laminar flow separation and subsequent turbulent reattachment. The thin laminar boundary layers upstream of this separation "bubble" were difficult to measure, so that the total-pressure profiles were only measured for turbulent boundary layers.

The trailing edge boundary layers on both the suction and pressure surfaces of a compressor cascade blade (c = 203.2 mm and Re_c = 478,000) were measured with a hot-film probe by Hobbs, Wagner, Dannenhoffer, and Dring [1980]. The two profiles are very detailed and precise; they show a nearly separated profile on the suction surface, and also a pressure surface profile typical of favorable pressure gradients.

Recently, Hodson [1983] has presented blade boundary layer data measured in a turbine cascade (c = 114.5 mm and Re_c = 315,000) with a hot-wire probe. Although no data points are reported, the velocity profiles on the suction surface show laminar flow until 78% chord followed by laminar separation and no reattachment.

All prior investigations have used hot-wire or pressure probes to make boundary layer measurements. There are three potential problems: first, a periodic two-dimensional cascade flow is difficult to establish and the probe may distort it; second, some boundary layers are likely to be small compared to the probe dimensions (some may be small relative to the LDV measurement volume, see Section IV); and third, separated regions, if present, cannot be conveniently studied. For these reasons, the current study used the LDV

technique. Before discussing the LDV results, however, we will describe the cascade facility and flow.

III. CASCADE TESTS

The cascade wind tunnel has a 0.37 m by 0.64 m test section with a maximum air speed of approximately 35 m/sec. Tunnel turbulence control is through a honeycomb with a 3.18 mm cell size, several settling screens in the diffuser section, and a nine-to-one contraction. Over the speed range of 24-35 m/sec, the tunnel operated with a freestream turbulence level of 0.18% ±10% as measured by a hot-wire anemomenter. Figure 1 shows a schematic of the open return facility.

The blade section used in the tests is a compressor blade designed at the NASA Lewis Research Center (see Sanger [1980]). The blade section is a double circular arc blade with 65 degrees of camber* and a 228.6 mm chord length. Both the leading and trailing edges were machined to a 9.14 μm radius. The blade aspect ratio is 1.61. The five cascade blades were made of aluminum and were anodized black to minimize laser reflections. Camber line and thickness relationships necessary to construct the blades (or for computation) are given in the Appendix. To insure proper alignment, the blades were carefully positioned in two inserts (aluminum and plexiglass** (on the optics side)), which were in turn mounted to the plywood walls of the cascade test section. The test section is shown in Figure 2. For the case to be reported, the cascade had a solidity of 2.14. The stagger angle was 20.5 degrees. The important cascade and flow angles are defined in Figure 2.

---

* A design condition was that the blade show some trailing edge separation of the suction surface turbulent boundary layer at zero incidence angle. With the available cascade geometry, this leads to a large camber angle.

**A glass insert was later placed within the plexiglass to improve the LDV signal.

As current computer codes assume a two-dimensional periodic cascade flow, one must take data in such a flow field for it to be of use. Two-dimensionality, of course, implies that the velocities and angles of the flow are substantially the same in spanwise planes, while periodicity supposes that velocities and flow angles show only minimal variations from blade passage to blade passage, both upstream and downstream of the blade row. For the five-bladed cascade used here, periodicity was taken to mean periodicity over three blade passages centered at the minimum velocity point of the middle blade wake. In order to satisfy the condition of continuity for a two-dimensional, incompressible cascade flow, the axial velocity must be held constant throughout. From a practical standpoint then, flow periodicity and two-dimensionality could be determined, for a uniform inlet flow, by examining the axial-velocity ratio and flow angles determined at the exit plane. This was quite useful as these outlet measurements could be made simply and quickly, thus allowing us to check the cascade flow daily.

Two-dimensionality and periodicity are normally controlled in cascades by using continuous suction over the entire blade pack.* Continuous suction was not possible in the current experiment because of the need for laser access. Alternate flow control was examined in some detail. Returning to Figure 2, we note that there are many potentially useful flow controls. That is, it is possible in principle, to control the flow by adjusting the position of the lower false blade, the upper false blade, the variable diffuser, and the tailboards (as well as the relative position of the tailboards), or by adjusting the magnitude (and distribution) of the top suction, side suction, and lower and upper channel suction. In practice, the lower and upper false

---

* Note that the control here seems to be over the growth of channel corner disturbances. An attempt to use a slightly divergent wall, commonly used to compensate for boundary layer growth, failed.

blades were each set at nominally one blade spacing from blades 1 and 5, respectively. The diffuser was set to minimize the flow angle at the splitter plate. Lower channel suction was not required. Top and upper channel suction were provided through the same 5 hp blower, which was run at full power. A baffle system was used to adjust the relative amounts of suction provided at the top and upper channel, and the baffling along with slight adjustments to the upper false blade position were used to insure a horizontal flow at the upper false blade leading edge. The tailboards were most useful in controlling the relative exit angles of the flow; that is, they could be adjusted so that the exit angle across the cascade in a blade-to-blade direction was constant outside of the wake regions. The periodicity, however, was found to be most influenced by the amount and distribution of the sidewall suction. Side suction was provided by a 10 hp centrifugal blower operated at full power. Side suction distribution was controlled by a complex baffling system. Six suction ducts were located at a half blade spacing on either side of each of the blades. Each of the individual ducts had a separate baffle control, and was adjusted by the simple but tedious procedure of changing a baffle position and then examining the resulting outlet flow. Presumably, the control of side suction distribution controlled the size of the sidewall boundary layer at its intersection with the blade pack leading edge line--in a sense controlling the virtual origin of the corner disturbances. Control of sidewall suction distribution then implied a control of the "blockages," caused by corner disturbance contamination, of each blade passage individually and hence control of the individual blade angles of attack. Once set, the stability of the periodicity obtained on a day-to-day basis was excellent.

The two-dimensionality and periodicity of the cascade flow were determined by conducting measurements of the cascade inlet and outlet velocity

profiles using five-hole probes. These probes are capable of resolving the three components of velocity as well as the relative yaw and pitch angles of the flow. Treaster and Yocum [1979] give a complete description of the five-hole probes employed in the study. The probes were calibrated at a speed of 30.5 m/sec in an open jet air facility over the range of pitch and yaw angles of +30 degrees to -30 degrees. Reynolds number effects on the probes have been shown to be small (see Treaster and Yocum [1979]).

All inlet and outlet five-hole probe surveys were referenced to a Pitot-static probe located 25.4 mm upstream of the blade pack leading edge line. The probe protruded approximately 150 mm into the flow--well outside of the sidewall boundary layer. The probe was located along a parallel to the leading edge line at a position between blades 3 and 4 at which the inlet velocity was roughly equal to the average of the measured inlet velocities.

Cascade inlet flow profiles were documented by five-hole probe measurements approximately 38 mm upstream of and parallel to the leading edge line. Outlet flow profiles were measured parallel to the trailing edge line and one-half chord downstream of this line. A nearly real-time data acquisition/reduction system was used for the velocity measurements. In each case the five-hole probe and Pitot-static probe data were sent to seven separate pressure transducers. These seven pressure signals as well as a test section temperature signal were scanned by a multiplexer/scanner, smoothed on a multimeter through a 100 cycle (1 2/3 sec) integration, and sent for reduction to a VAX 11/782. Velocities, velocity ratios, and flow angles could be displayed on a video terminal, written on a line printer, or plotted on a flat-bed plotter.

Inlet velocity surveys were made after the outlet flow had been determined to be satisfactory. Good periodicity and spanwise consistency were apparent, as was some streamline bending induced by the presence of the

blades. An average inlet velocity was found to be 33.11 m/sec, with an average incidence angle of 5 degrees. Chord Reynolds number, based on the inlet velocity, was 500,000 with an observed ±1% variation on a day-to-day basis. Figure 3 shows a typical outlet flow profile and the equivalent turning angles. The periodicity of the flow is clearly excellent. The axial-velocity ratio is determined by averaging the local axial-velocity ratio over three blade passages, centered at the minimum velocity-ratio point of the center blade wake. In the calculation, the inlet flow is assumed to be spatially constant at its average value (the Pitot-static tube reading). The average axial-velocity ratio was found to be 1.0; on a day-to-day basis the variation was within ±3%. The flow turning angle averaged across the three center blade passages was 54 degrees. Figure 4 shows all of the blade geometry and the inlet and outlet flow measurements.

Measurements have been taken to help quantify the losses in total pressure across the cascade. Additional quantities can be computed to compare with design limits on diffusion rate and static-pressure rise within the cascade. The difference between the blade-passage-averaged flow angle in the outlet flow and the exit blade "metal" angle is the deviation angle. For the current study, the deviation angle was measured to be 16 degrees, which is very large.* Non-dimensionalizing by the inlet dynamic pressure, the blade-passage-averaged total-pressure loss coefficient was 0.151 and the blade-passage-averaged static-pressure rise coefficient was 0.463. Note that the static-pressure rise coefficient was probably affected by the positioning of the tailboards. An equation for the total-pressure loss coefficient was developed by Lieblein and Roudebush [1956] where

$$\bar{\omega} = 2\left(\frac{\theta}{c}\right)\frac{\sigma}{\cos\beta_2}\left(\frac{\cos\beta_1}{\cos\beta_2}\right)^2\left[1-\left(\frac{\theta}{c}\right)\frac{\sigma H_{12}}{\cos\beta_2}\right]^{-3}\left(\frac{2H_{12}}{3H_{12}-1}\right) \quad .$$

*Although large, a 16 degree deviation angle is not unexpected, as the design condition called for a zero incidence angle. Experiments at lower incidence angles are planned.

A value of 0.172 for $\bar{\omega}$ can be calculated from this equation using the flow parameters measured in the outlet flow. The loss in total pressure across the cascade is related to the amount the flow is diffused through the blade passage. Lieblein, Schwenk, and Broderick [1953] derived a diffusion factor where

$$D = 1 - \frac{V_2}{V_1} + \frac{V_{\theta_1} - V_{\theta_2}}{2\sigma V_1} = 1 - \frac{\cos \beta_1}{\cos \beta_2} + \frac{\sin \beta_1 - \cos \beta_1 \tan \beta_2}{2\sigma} \quad .$$

Designers normally place a limit of 0.6 on D when designing a blade row. This limit is based on a large number of cascade performance tests. Values of D greater than 0.6 result in large increases in total-pressure loss because the larger amount of diffusion causes the blade boundary layers to separate. Using a blade-passage-averaged value of the outlet flow angle allows a value of 0.658 for D to be computed for the current study. This value of D indicates a risk of separation.

Ideally, blade static pressure would be measured on the center blade of the cascade--the one intended for LDV measurements--but the two types of measurements had somewhat conflicting requirements. That is, an aerodynamically smooth (0.8 μm estimated surface roughness) surface was desired for the LDV surveys, while the conveying tubes required for the pressure measurements inevitably led to a somewhat roughened surface. To work around this problem, we instrumented the suction surface of the upper blade, 4 (see Figure 2), and the pressure surface of the lower blade, 2, with 24 pressure taps; we instrumented the center blade, 3, pressure and suction surfaces with 6 and 7 taps, respectively. Since the flow was periodic, the

pressure distribution could be obtained from blades 2 and 4 as well as from blade 3. After checking this by comparing the results of the pressure distributions from blades 2 and 4 against the data from blade 3, (the agreement was excellent), we interchanged blade 3 with the uninstrumented blade, 5, for the LDV surveys. Data acquisition and reduction, for the static-pressure distribution, were similiar to that described for the five-hole probe data with the exception that a scanner valve was used to switch the pressure data, hole-by-hole, to a single transducer during data acquisition.

The blade static-pressure distribution appears in Figure 5. Integrating this distribution gives a lift coefficient of 0.952. The 5 degree incidence angle dramatically affects the pressure distribution. The large favorable gradient on the pressure surface suggests that the boundary layers near the leading edge will be laminar; transition should be looked for on the pressure surface. The unfavorable gradient at the leading edge of the suction surface implies a leading edge separation. The rather flat pressure profile near the trailing edge of the suction surface suggests that the flow may be separated there. The rapid and continuous changes of pressure on both the pressure and suction surfaces offer little hope of finding equilibrium boundary layers. In addition, the inviscid velocity field within the blade passage will be under the influence of a normal pressure gradient, and one cannot anticipate a constant freestream velocity region.

Following the sublimation method used by Holmes and Obara [1982], we used surface flow visualization to help determine the location of the anticipated trailing edge separation on the suction surface, and the transition on the pressure surface. An air brush was used to coat the blade with a mixture of napthalene and acetone in a 1:8 solid-to-solvent volume

ratio. Preliminary tests determined that a run time of nine minutes was sufficient to set up the visualization pattern. For each run the center blade was removed, the napthalene/acetone mixture was applied, and large particles were dusted off. The blade was then replaced in the cascade and removed after the nine minute run time, allowing the sublimation pattern to be photographed. A sufficient number of tests were taken so that a meaningful mean and Student's t test deviation could be obtained. Evidence of two-dimensionality was much more apparent in the suction surface separation pattern then in the pressure surface transition pattern. This is perhaps an indication of the importance of the local surface roughness in determining the transition point for the very thin boundary layers encountered. With 95% confidence, separation was found to occur at 65.6% chord on the suction surface with a deviation of ±3.5% chord. Transition was found on the pressure surface to be at 64.2% ± 3.9% chord to the same level of confidence.

IV. THE LASER DOPPLER VELOCIMETER

All blade boundary layer and near-wake measurements were made using a single-component LDV. For all the LDV measurements, a specially designed traversing mechanism was used which matched the arc of motion of an optics cradle to that of the blade curvature (two arcs were employed, one for each of the pressure and suction surfaces). All measurements were made in the plane of the local blade normal. Translation of the optics cradle normal to the blade could be accomplished in step intervals as small as 0.0254 mm. Prior to the LDV measurements, a reference distance was established by focusing the LDV control volume on an insert which securely fit over the center measuring blade. Narrow lines had been etched on the insert (on arcs matching the blade curvature) to be known distances from the blade surface. Repeatability in

establishing a measurement reference was estimated to be ±0.05 mm, and this uncertainty is probably the major source of scatter in the velocity data.

A two-watt, Spectra-Physics, Argon-Ion laser was used for the measurements. Power on the blue line (488 nm wavelength) ranged between 0.5 watts and 0.7 watts on a day-to-day basis. Standard TSI backscatter optical components were used: the 371.3 mm focusing lens was chosen to allow the measurements to be made at the blade midspan. The ellipsoidal measurement volume was reduced through the use of a (2.71:1) beam expander; the predicted measurement length in the normal to the blade direction was 37 μm. While this length was small when compared to the length scales of the turbulent boundary layers on the suction surface, we shall show that it is roughly half the size of the displacement thickness of the initial laminar profile on the pressure surface. Where appropriate, optical shifting at 5 MHz was employed. Note that to measure close to the blade surface the optical cradle was tilted at an angle of roughly 1 degree. Silicon carbide particles having a mean diameter of 1.5 μm were used for laser seeding. In an attempt to maintain a uniform distribution, we injected the silicon carbide particles well upstream of the measurement station at the flexible coupling (see Figure 1). The particles were suspended in a "cloud chamber," which was constructed for this study, and were injected into the tunnel by a small overpressure. Gain, on the counter processor, was kept low, and particle counts averaged only 20 or so particles per second (as we will discuss, however, the velocity probability distributions were remarkably clean).

LDV data acquisition and reduction was accomplished by using a direct link to a Vax 11/782 computer. Software allowed selection of the focusing lens half angle, the laser wavelength, the frequency shift, the minimum number of cycles employed in the calculation (8 here), and the number of particle

counts per run. Initial output was in the form of a velocity histogram. Minimum and maximum velocity limits could be set by two cursors to eliminate obvious noise from the distribution. Final output was mean velocity, local turbulence intensity, and the percent of particle counts employed in the calculations. For some of the profiles measured the skewness and kurtosis of the distribution were also calculated. The percentage of particle counts employed in the calculation may be used as an indicator of signal-to-noise ratio. At least 98% of the total particle counts were used for measurement stations in the boundary layer; at least 95% were employed for points in the freestream (the difference in percentages reflects the fact that fewer overall points were used at the freestream locations).

For a counter processor, employed in a highly turbulent flow, the calculation of mean velocity and turbulence intensity may not be straightforward. McLaughlin and Tiederman [1973], Hoessel and Rodi [1977], Giel and Barnett [1979], Edwards [1981], Edwards and Jensen [1983], Johnson, Modarress, and Owen [1984], and Stevenson, Thompson, and Craig [1984] have all discussed the question of velocity bias in a highly turbulent flow. As pointed out first by McLaughlin and Tiederman [1973], the problem arises because more high-speed particles than low-speed particles arrive in the measurement volume during a given measurement interval. A related problem, termed incomplete signal bias by Stevenson, Thompson, and Craig [1984], can be eliminated by employing a sufficiently high frequency shift.

McLaughlin and Tiederman [1973] describe a correction for the phenomenon (with uniform seeding)--but it requires complete velocity vector information. A more practical one-dimensional correction is also given, but this correction tends to overestimate the error for local turbulent intensities >20%. Edwards

[1980] shows that the biasing error can be made negligibly small for the case of a saturated data handling system (taking data at a fixed rate set by the slowest component of the system) by taking the particle density equal to the seeding rate (this assumes a validation circuit for the system). Stevenson, Thompson, and Craig [1984] used equal time interval sampling in a very highly seeded mixing layer as a bias-free test case. As pointed out by Edwards and Jenson [1983], however, very high seeding rates may open the door to other types of errors, for example, by reducing the actual number of statistically independent samples used to form the velocity statistics. Moreover, a very high-seed rate may be very difficult to achieve in precisely those regions in which the bias is expected to be high. Often, in fact, a counter processor is chosen over a tracker processor because of its ability to act at very low seeding rates.

The bias question is obviously quite complex, and a consensus opinion on how to correct data is still lacking. Some issues, such as non-uniform particle seeding, of interest particularly in air flows, have not yet been the subject of detailed studies (see Hoessel and Rodi [1977] for instance). Giel and Barnett [1979] conducted an experiment favorable to obtaining statistical bias, but no consistent bias was evident--thus further obscuring the bias question. In the current study, we employed simple arithmetic averaging. For many of the boundary layers measured, we monitored the skewness with the idea that a change of shape from the classical distribution in the boundary layer might signal significant velocity bias. No such deviations were observed. We note that both Mclaughlin and Tiederman [1973] and Johnson, Modarress, and Owen [1984] show that the overestimate of the mean velocity goes roughly quadratically with turbulence intensity, being 5% for a local turbulence

intensity near 20%, and being 12% for a local turbulence intensity near 35%.* These numbers should be borne in mind not only when evaluating the data presented here, but also when evaluating any measurements made in highly turbulent flows. The mean velocity here was taken as

$$u = \frac{1}{N} \sum_{n=1}^{N} u_n \quad ,$$

the local turbulence intensity was taken as

$$\frac{u'}{u} = \frac{1}{u} \left[\frac{1}{N} \sum_{n=1}^{N} (u_n - u)^2 \right]^{1/2} \quad ,$$

and the turbulence intensity was taken as u'/U_e.

Experience has shown that quite satisfactory repeatability of the mean velocity and turbulence intensity can be guaranteed in boundary layer flows by using 1000 particle counts in regions in which the local turbulence intensity exceeds 5%. In regions of local turbulence intensity of less than 5% but more than 2%, 500 points are used, while 200 points are used in regions of less than 2%. At each chord position, profiles were defined by statistically treating the data for six individual experiments. Six experiments were chosen as the statistics found from six experiments showed less than 1% scatter in the freestream data. Error bands, presented on the LDV data plots, represent 95% confidence levels as determined by a Student's t test.

The preliminary data analysis is automated on the VAX 11/782 computer. The effect of the normal pressure gradient on the boundary layer profiles is accounted for first. Details of the technique are given by Zierke and Deutsch [1985] and basically follow the approach suggested by Mellor and Wood [1971]

---

*It is not obvious that turbulence intensity is the only relevant variable. For example, the values of the higher moments of the velocity probability distribution are no doubt also of importance.

and Ball, Reid, and Schmidt [1983]. Briefly the technique assumes that the profile may be represented as

$$u = u_{meas} - u_{inv} + U_e$$

so that the edge velocity (U_e) can be determined by extrapolating the outer inviscid flow (u_{inv}) to the wall (where $u = u_{meas} = 0$) in some reasonable manner. The method is not rigorous in its definition of the inviscid region, and hence in the manner of extrapolation. Our own experience with the 22 boundary layers measured here, however, is that the edge velocity is quite insensitive to any reasonable choice of the inviscid region.

V. PRESSURE SURFACE BOUNDARY LAYERS

Boundary layer measurements were made at 11 chord locations on the pressure surface of the center cascade blade. To help interpret these velocity profiles, Figure 5 shows the measurement locations along with the pressure distribution. The combination of continuously changing pressure and moderate surface curvature ($0.002 < |\delta/R_c| < 0.02$) signals a complicated non-equilibrium flow field. At the leading edge, for example, the large incidence angle (5 degrees) results in a strong acceleration which promises a region of laminar flow. In the region from 8% chord to 62% chord, the flow is subjected to a mildly adverse gradient so that the onset of transition might be expected in this region. The subsequent favorable gradient, however, makes the eventual complete transition to turbulence problematic.

The measured pressure surface boundary layers are shown in Figure 6.* The blade-to-blade pressure gradient affects the inviscid region of each profile. This pressure gradient varies from a strong, non-linear gradient near the leading edge, where the streamlines have a large curvature, to a nominally

---

*Tabulated data will be supplied upon request.

zero gradient near the trailing edge. As previously noted, each profile was measured six times and the symbols in Figure 5 represent velocity data averaged over the six tests. The error bands give 95% confidence levels as determined by the Student's t test. These error bands are quite small, particularly in the inviscid regions. The exception appears at 2.7% chord where the boundary layer is so small that the LDV could only nominally penetrate the layer, and correspondingly, the resolution is poor.

The boundary layers were analyzed using methods described by Zierke and Deutsch [1985]. The influence of the normal pressure gradient was first removed. The reconstructed boundary layer data were then compared with a Falkner-Skan velocity profile (see Falkner and Skan [1931]) at the local streamwise pressure gradient. For the velocity profiles measured near the trailing edge, an attempt to fit the results to the wall-wake equation of Coles [1956] was also made. Finally, integral parameters were obtained from both a smoothed cubic spline fit of the data and from the Falkner-Skan solutions. The velocity profiles are replotted non-dimensionally in Figure 7. In spite of the influence of both curvature and changing pressure gradient on the flow field, the Falkner-Skan approximation appears to reasonably represent the mean velocity profiles through about 57.2% chord. At 68.0% chord and beyond, there is an increased thickening of the measured profiles relative to the Falkner-Skan correlation which indicates transitional boundary layers.

Empirical relationships have been developed for the prediction of the beginning and end of transition; these relationships include the effects of freestream turbulence and streamwise pressure gradient. Using the relationships of Abu-Ghannam and Shaw [1980], for example, we predicted the onset of transition for the pressure surface data using the measured

pressure distribution and a freestream turbulence intensity (in the blade pack) of 1.5%. This turbulence intensity value was determined from hot-wire measurements at the edge of the boundary layer, close to the blade leading edge. Onset of transition was predicted to be at a momentum thickness Reynolds numbers (Re_θ) of 342, and comparison with the Re_θ found from the profiles put this onset at 47.8% chord. By onset here, we mean the first location at which the intermittency, as measured with a flush-mounted film probe for example, would be greater than zero. Because of the strong favorable gradient near the trailing edge, the scheme also predicted that a fully-turbulent boundary layer would not develop on the pressure surface. There do not seem to be any empirical prediction schemes which include the effect of surface curvature. While convex curvature apparently has no effect on transition, the concave curvature of the pressure surface can promote the generation of Görtler vortices (see Görtler [1940]), which can cause transition to occur earlier.

Sublimation flow visualization studies helped determine the transition point on the pressure surface. The average of five flow visualization tests placed the transition point at 64.2% ± 3.9% chord with 95% confidence. Figure 8 shows a plot of mean velocity, normalized by the edge velocity, for a fixed distance (y = 0.508 mm) above the plate and a varying chord location. At this distance above the surface, the measurement volume is above the boundary layer for the first two chord locations. The decrease in mean velocity with chord location over the first half of the blade reflects the growth of the boundary layer relative to the fixed distance. The rapid rise in mean velocity near 60% chord indicates the onset of transition (see for example, Klebanoff, Tidstrom, and Sargent [1962]). Agreement with the flow visualization studies appears to be quite good. However, the simple empirically based calculations

of Abu-Ghannam and Shaw [1980] pick too small a chord value for the onset of transition. The fact that the mean velocity does not reach a constant (or decreasing) value with increasing chord location indicates that the transition process is not complete.

Integral parameters can also characterize transitional boundary layers. Plots of displacement thickness (δ^*), first shape factor (H_{12}), and Re_θ are shown in Figure 9. Also shown are values for the skin friction coefficient (C_f). Most of the integral parameters shown in Figure 9 were obtained from the smoothed cubic spline approximation. Because of the lack of near wall measurements for some of the extremely thin layers, we felt that the values of momentum thickness obtained from the spline fit were not accurate, so that some values of H_{12} and Re_θ (as shown in Figure 9) were calculated from the appropriate Falkner-Skan appoximations. Note the large decrease in δ^* as the flow encounters the favorable pressure gradient near the trailing edge. H_{12} shows laminar-like values until just before the 68.0% chord location, at which point the values drop into the turbulent regime. The values of C_f are determined from the Falkner-Skan approximations. At the leading edge, the skin friction goes to infinity. In the transition regime, the C_f values, although known to increase, cannot be easily estimated. To indicate how large C_f might become near the trailing edge, a value based on the Ludweig-Tillman empirical expression (see Ludweig and Tillman [1949]) is given for the 97.9% chord location. Use of the Ludweig-Tillman expression here is not strictly valid, as the boundary layer profile is probably not fully turbulent at 97.9% chord.

An attempt was made to fit the boundary layer profile at 97.9% chord to the wall-wake equation, but no logarithmic region was obtained. Purtell, Klebanoff, and Buckley [1981] concluded that the logarithmic region seems to

be an inherent characteristic of the turbulent boundary layer. That is, for fully-developed turbulent boundary layers, they found the extent of the logarithmic region to be roughly a constant fraction of the boundary layer thickness as Re_θ was decreased. Murlis, Tsai, and Bradshaw [1982] found strong evidence for the validity of the logarithmic law of the wall, at zero pressure gradient, for Re_θ values as low as 700, while Smits, Matheson, and Joubert [1983] found a logarithmic region, for favorable pressure gradients, at Re_θ as low as 261. Since no logrithmic region was found for the boundary layer at 97.9% chord, it must be concluded that either the boundary layer was not fully turbulent at a Re_θ of 388, or (less likely) that the logarithmic region was so small that it could not be detected.

Turbulence intensity data for the pressure surface boundary layer are shown in Figure 10. As the Falkner-Skan approximation has been shown to be reasonable for the profiles to 57.2% chord, the large turbulence intensities near the wall are disturbing. A typical profile of the skewness versus y/δ^*, which is shown for the 5.9% chord location in Figure 11, adds considerably to the problem in that this profile might reasonably resemble the shape of a skewness profile one might expect to find from measurements of a turbulent boundary layer.

This problem was examined in some detail. Using both calibrated hot-wire probes in the boundary layer and uncalibrated hot films flush-mounted on the surface, we determined that the profiles near the leading edge were indeed laminar. Typically, at the edge of these leading edge boundary layers, the intensity was found to be near 1.5%. The difference between this value and the 0.18% found in the approach flow is probably due to the interaction of the flow with the blade pack. Having shown the boundary layers to be laminar, we next suspected that the intensity measurements might be contaminated by

mean-velocity-gradient broadening. This problem has been considered previously by Edwards, Angus, French, and Dunning [1971], Goldstein and Adrian [1971], and Kried [1974]. For simplicity in the current study, the laser intensity was taken to be constant for the entire measurement volume. In the present case then, error estimates could be easily made by assuming the Falkner-Skan approximate profiles or by using the smoothed cubic spline fit. Similiar results are obtained for either estimate. In Figure 12a, an estimate of the turbulence intensity caused by mean-velocity-gradient broadening is shown against percent chord for a measurement volume roughly as large as the volume estimated in Section IV. As it seemed plausible that the actual measurement volume might be larger than the volume estimated theoretically, we repeated the calculations for a measurement volume roughly twice that of the estimated volume. These results are shown in Figure 12b. Figures 12a and 12b show estimates for a constant y/δ^* of roughly 1.70; the measurement points are also given. It is clear from a comparison of the turbulence intensity calculated from the velocity-gradient broadening against the measured data, that gradient broadening alone cannot account for the entire intensity. In addition, the skewness when calculated from an assumption of velocity-gradient broadening is much smaller than that observed experimentally.

As a second approach to the problem, we assumed that in addition to the gradient broadening problem, a small vibration may have contaminated the velocity signal. Calculations are again straightfoward using either the spline fit or the Falkner-Skan approximations. Results for vibration amplitudes of 25.4 μm and 50.8 μm are again given in Figure 12. With the exception of the points at 5.9% chord, which appear to have been biased by an inaccurate calculation of δ^* (see Figure 9), the calculations agree reasonably well with the measurements for a measurement volume of 66 μm and a vibration

amplitude of 50.8 μm. Comparison between the measured and calculated skewnesses are also much closer. Some simple measurements with an accelerometer indicated that vibration amplitudes of this magnitude were not unreasonable to expect, so that a combination of velocity-gradient broadening with a vibration of the measurement volume seems a likely cause for the elevated turbulence levels. As shown in Figures 12a and 12b (and as can be shown for the suction surface turbulent profiles), the effect becomes quite small as the boundary layer grows. In the present situation, the bias can probably be considered negligibly small for chord positions larger than about 25%.

Turbulence intensity profiles are shown for the transitioning boundary layers on the pressure surface in Figure 10. The data show classical shape (see Klebanof, Tidstrom, and Sargent [1962]) and agree reasonably well with the measurements of Wang, Simon, and Buddhavarapu [1985].

VI. SUCTION SURFACE BOUNDARY LAYERS

Suction surface boundary layers were taken at 11 chordwise locations on the center blade. Figure 5 shows these chordwise locations as well as the static-pressure distribution. A very large adverse pressure gradient exists near the leading edge. This gradient gradually becomes less severe with downstream distance and vanishes entirely near 80% chord. No pressure gradient is evident the last 20% of the chord which indicates a possible separation region--that is, a region which cannot sustain a streamwise pressure gradient.

The measured suction surface boundary layers are presented in Figure 13. As was the case for the pressure surface boundary layers, the inviscid regions show the effects of the normal pressure gradient. For the suction surface, however, $\partial p/\partial y > 0$ as opposed to the pressure surface where $\partial p/\partial y < 0$. Once

again, the large curvature in the streamlines near the leading edge results in a highly curved inviscid region. The 95% confidence bands are quite small for all the boundary layers except in two regions. First, the thin boundary layer at 2.6% chord has a large velocity gradient near the surface; because of this large gradient, the sensitivity to probe placement is heightened, and the measurements are less repeatable. Second, as suspected, the boundary layer at 94.9% chord was separated, and the unsteadiness in the separation process resulted in larger error bands.

All of the measured suction surface boundary layers are turbulent. This implies that transition took place before the measurement station at 2.6% chord, which is not surprising considering the very large adverse pressure gradient near the leading edge. The separation of a laminar boundary layer under an adverse pressure gradient results in a free shear layer, which is unstable. The transition to turbulence takes place very rapidly. Once turbulent entrainment increases, the shear layer is enlarged which results in a pressure recovery and a rapid reattachment. Thus, the separation "bubble" can be quite short and close to the leading edge.

Although the transition takes place very close to the leading edge, the recovery process extends some distance downstream. This process can be seen from the mean-velocity profiles plotted in dimensionless outer variables. These plots are shown in Figure 14 where the normal pressure gradients have been taken into account as described previously (see Zierke and Deutsch [1985]). The recovery process can be seen to extend through the 2.6% and 7.6% chord locations by observing the shape of the profiles. As we will show later, the shape of the velocity profiles results in higher values of H_{12} during the recovery process. The local turbulence intensity profile at 2.6% chord also indicates recovery. This turbulent boundary layer was the only one

measured in which there was a maximum value of local turbulence intensity away from the surface.

The mean velocity data were fit to the wall-wake equation of Coles [1956],

$$\frac{u}{u_\tau} = \frac{1}{\kappa} \ln\left(\frac{y\ u_\tau}{\nu}\right) + C + \frac{\Pi}{\kappa} W\left(\frac{y}{\delta}\right) \quad ,$$

through a least squares technique described by Zierke and Deutsch [1985]. For a given boundary layer thickness, the technique simultaneously calculates the values of u_τ and Π which yield the best fit to the data. Figure 15 shows the velocity profiles in inner variables. The logarithmic region reaches a maximum and the wake region reaches a minimum at 12.7% chord. This seems to be a second indication of complete recovery from the leading edge separation "bubble." Moving further downstream, Coles' wake parameter, Π, (which controls the size of the wake region) and Re_θ increase resulting in a reduction in the extent of the logarithmic region. As separation is reached, the logarithmic region disappears and the wall-wake equation cannot be fit to the data. This conclusion was reached earlier by Simpson, Strickland, and Barr [1977], who found the law of the wall valid until intermittent separation (flows containing instantaneous flow reversals) was reached.

Although the influence of surface curvature cannot be extracted from the data, one must suspect that this influence is indeed present. The convex curvature on the suction surface ($0.01 < |\delta/R_c| < 0.2$) and the concave curvature on the pressure surface ($0.002 < |\delta R_c| < 0.02$) have opposite effects on turbulent boundary layers. Ramaprian and Shivaprasad [1977] show that convex curvature reduces the logarithmic region and increases the relative strength of the wake component. Except for the initial region of curvature, convex curvature increases the rate of growth of Re_θ and decreases C_f. Shivaprasad and Ramaprian [1978] claim that the effects of convex curvature on

the behavior of the turbulent boundary layer are even stronger than the effects of concave curvature at the same value of $|\delta/R_c|$. Their measurements showed that convex curvature reduces turbulence intensity and Reynolds shear stress. Measurements by So and Mellor [1973], Gillis and Johnston [1983], and Gibson, Verriopoulos, and Vlachos [1984] agreed. These results indicate that for very strong convex curvature effects, regions can be found where turbulence cannot exist. Bradshaw [1969] showed that the behavior of the turbulent boundary layer is very sensitive to streamline curvature as mild as $|\delta/R_c| = 0.003$. He used an analogy between the effects of streamline curvature and buoyancy to estimate quantitatively the effect of curvature on mixing length distribution in the boundary layer. So [1975] verified this buoyancy analogy mathematically. Shivaprasad and Ramaprian [1978] made measurements which support the buoyancy analogy of Bradshaw [1969] for mild convex curvature. For concave curvature, they found the bouyancy analogy useful only for values of $|\delta/R_c|$ near 0.01.

Figure 16 includes plots of δ^*, H_{12}, Re_θ, and C_f. These parameters were calculated from a smoothed cubic spline fit of the data, except for C_f, which was calculated from the least squares fit of the data to the wall-wake equation. Values of H_{12} and Re_θ were also used to calculate C_f from the empirical equation of Ludweig and Tillman [1949]. The displacement thickness increases gradually at first and then increases rapidly through separation. The plot of H_{12} indicates a turbulent boundary layer beginning near the leading edge. Recovery from the leading edge separation "bubble" results in an initial decrease of H_{12}. Separation of turbulent boundary layers is usually approximated using values of H_{12} near 2.2 which corresponds here to a suction surface location near 60% chord. Sandborn and Kline [1961] proposed a relation for intermittent separation,

$$H_{12} = 1 + \frac{1}{1 - \frac{\delta^*}{\delta}} \quad ,$$

which yields 66.9% chord (corresponding to $H_{12} = 2.70$) as the location of intermittent separation for the data presented here. Values of C_f appear to be near zero at the leading edge which corresponds to the vanishing skin friction at the beginning of the leading edge separation "bubble." C_f reaches a maximum after the boundary layer has totally recovered from the leading edge separation and then decreases as the trailing edge separation of the turbulent boundary layer is reached. C_f vanishes near 80% chord.

Defining separation as the entire process of the breakdown of boundary layer flow, Simpson, Chew, and Shivaprasad [1981] quantified the various stages of separation with the instantaneous backflow near the wall. Incipient detachment (ID) occurs with 1% instantaneous backflow; intermittent transitory detachment (ITD) occurs with 20% instantaneous backflow; transitory detachment (TD) occurs with 50% instantaneous backflow; and detachment occurs when the wall shear stress becomes zero. The percent backflow is easily calculated as the portion of the measured velocity distribution that includes negative velocities. Figure 17 shows the instantaneous backflow measurements at the 63.2%, 74.0%, 84.2%, and 94.9% chord locations. Figure 18 shows the maximum percent backflow as a function of percent chord. The sublimation flow visualization tests showed separation to occur at 65.6% ± 3.5% chord, and a comparison with the maximum instantaneous backflow data of Figure 18 shows that flow visualization yields a value for separation which is only slightly downstream of incipient detachment. Locating turbulent separation by observing when H_{12} nears 2.2 also seems to indicate incipient detachment. We might note that although Simpson, Chew, and Shivprasad [1981] state that

detachment and transitory detachment need not be at the same location, our skin friction calculations show that the chordwise locations of detachment and transitory detachment are quite close to one another.

Restrictions in applying the wall-wake equation in the vicinity of separation result from the velocity scale, u_τ, approaching zero. A vanishing u_τ leads to a vanishing logarithmic region, which would not cause concern if the separated flow profiles would follow the law of the wake. Unfortunately, experimental data prove otherwise (see Simpson, Chew, and Shivaprasad [1981] for example). Perry and Schofield [1973] developed a similarity defect law based on the maximum shear stress rather than the wall shear stress. The defect law was originally developed for attached boundary layers under moderate to strong adverse pressure gradients where $\tau_{max}/\tau_w > 1.5$. The defect law is

$$\frac{U_e - u}{U_s} = 1.0 - 0.4\left(\frac{y}{B}\right)^{1/2} - 0.6 \sin\left(\frac{\pi y}{2B}\right)$$

where

$$U_s = 8.0\left(\frac{B}{L}\right)^{1/2} U_m$$

and

$$B = 2.86\ \delta^*\left(\frac{U_e}{U_s}\right) \quad .$$

U_m is a velocity scale based on the maximum shear stress ($U_m = \sqrt{\tau_{max}/\rho}$) and L is the distance from the wall to τ_{max}. The velocity scale U_s is found using the methodology that Clauser [1954] used to determine u_τ. A half-power equation is used near the wall,

$$\frac{u}{U_e} = 0.47\left(\frac{U_s}{U_e}\right)^{3/2}\left(\frac{y}{\delta^*}\right)^{1/2} + 1.0 - \frac{U_s}{U_e} \quad .$$

Perry and Schofield [1973] suggested using the defect law for the outer 90% of the boundary layer with the half-power equation forming the innermost portion of that defect law. They recommended the law of the wall as an inner wall matching condition. Schofield [1983] extended the model to detached flows by suggesting that the similarity would hold provided that the origin of the normal coordinate has been moved from the wall to the location at which $u = 0$.

The suction surface boundary layers are plotted using the similarity relation of Perry and Schofield [1973] in Figure 19. In the outer 90% of the boundary layer, the similarity relation collapses the data quite well for chord locations upstream of the separated region. As the amount of instantaneous backflow increases, however, the data deviates more and more from the similarity relation. This deviation is in seeming contrast to the conclusions made by Schofield [1983]. A close examination of his defect plots, however, shows similar trends in his analyzed data and the data shown in Figure 19.

No outer region similarity seems to exist downstream of detachment. Many researchers have attempted a law of the wake correlation without success (see Simpson, Chew, and Shivaprasad [1981] for example). For a turbulent boundary layer subjected to a streamwise pressure gradient, Mellor and Gibson [1969] suggested replacing the shear velocity with a pressure velocity, $(\delta^*/\rho)(dp/dx)$, as the velocity scale. However, Schofield [1981] has shown this scaling to be inadequate. Using the velocity scale corresponding to the maximum shear stress as suggested by Schofield [1983] has been shown to give

poor similarity in Figure 18. Mehta and Goradia [1984] had some success by assuming the the outer region velocity profiles behave like a two-dimensional mixing layer. Their similarity variables were not found to give outer region similarity with the data measured here.

Similarity in the backflow region seems to show more promise. Simpson, Chew, and Shavaprasad [1981] found good backflow similarity by normalizing the velocity by the maximum backflow velocity, and the distance from the wall by the distance to the maximum backflow velocity. Schofield [1983] found that this backflow similarity could be improved by using the total backflow thickness as the length scale. Figure 20 shows this backflow similarity for the data at 94.9% chord. Despite the scatter, the backflow data seems to collapse quite well with the data measured by Simpson, Strickland, and Barr [1977] and Simpson, Chew, and Shivaprasad [1981]. The only exceptions are the two data points closest to the wall--data for which the 95% confidence bands are larger than the magnitude of the mean velocity.

The turbulence intensity on the suction surface is shown for all eleven chord positions in Figure 21. Recovery from the leading edge separation is apparent from the peaks in turbulence intensity that occur away from the surface for the 2.6% and 7.6% chord locations. These peaks also occur in the separation region from 63.2% chord through 94.9% chord. This shape reflects the movement in the location of the maximum mean-shear rate outward from the near-wall region.

VII. WAKES

Near-wake measurements were made at 105.4% chord and 109.6% chord using the LDV technique. Five-hole probes were used to measure the far wake at 152.6% chord. Figure 22 shows the data points and their 95% confidence bands for all three wake profiles. The two near-wake profiles, which are quite

similar, are very asymmetric because of the large difference in trailing edge boundary layer thicknesses on the two surfaces of the blade. The separation of the suction surface boundary layer leads to negative mean velocities at the center of the near wake. Other researchers have also measured negative mean velocities in near wakes. Wadcock [1980], using a flying hot wire, measured negative mean velocities in the near wake of an airfoil. Braden, Whipkey, Jones, and Lilley [1983] used a LDV to measure negative mean velocites in the near wake of an airfoil with confluent boundary layers.*

Wakes become similar only at distances far downstream of their source. A Gaussian distribution can be used to correlate these far-wake data. Lakshminarayana and Davino [1979] suggested the correlation

$$\frac{U_e - u}{U_e - u_{CL}} = e^{-0.693\ \eta}$$

where η is the normalized distance across the wake. The suction and pressure sides of the wake use different length scales, L_s and L_p. L_s and L_p are the distances on the suction and pressure sides of the wake centerline from the point of minimum velocity to a point where the velocity defect is $(U_e - u_{CL})/2$. The far-wake data of Lakshminarayana and Davino [1980] showed similarity away from the wake edge for both inlet guide vane wakes and stator blade wakes. This similarity was corroborated by Hobbs, Wagner, Dannenhoffer, and Dring [1982] for distances greater than 30% axial chord downstream of the trailing edge of their compressor cascade blades. Figure 23 shows that our wake data has Gaussian similarity in the far wake. However, the two near-wake profiles exhibit no similarity.

---

*Confluent boundary layers develop on an airfoil with leading edge slats or trailing edge flaps which causes the boundary layers from the various surfaces to interact.

Integral parameters can be calculated from the wake velocity profiles. Using the location of the wake centerline and displacement thicknesses on either side of the centerline, the displacement surface can be drawn as seen in Figure 24. The curvature of the displacement surface in the near-wake region can be explained by the pressure difference of the two blade surfaces. The location of the displacement surface in the far-wake region can be partly explained by the large amount of separation on the suction surface of the neighboring blades. However, the major explanation for this curvature of the displacement surface in the far-wake region is the confinment of the far wakes between the two tailboards (see Figure 2). The effects of the tailboards must be taken into account when considering this displacement surface for wake modeling.

Turbulence intensity profiles are presented for the two near wakes in Figure 25. As with the turbulence intensity profiles in the separating boundary layers, the turbulence intensity peaks are displaced outward, essentially tracking the regions of large mean-velocity gradients. These data, although more detailed, are quite similar to the data of Hah and Lakshminarayana [1982] for the near wake of an isolated airfoil.

VIII. CONCLUSIONS

Viscous calculations for turbomachinery applications have been handicapped by a lack of sufficiently detailed and precise data against which these calculation schemes can be compared. In order to help overcome this problem, we have presented measurements of the boundary layers and wakes about a double circular arc, compressor blade in cascade. A two-dimensional, periodic cascade flow has been developed without the use of continuous side wall suction. This facility has allowed these measurements to be made with a non-intrusive LDV system.

Despite the facts that the measured flow field was very complex and that only a one-component LDV system was used, the measurements presented here have led to an initial physical understanding of the cascade flow field. Regions of laminar flow, transition, recovery from a leading edge separation "bubble," non-equilibrium turbulent flow, separated flow, and near-wake flow have all been investigated. Prediction of a flow field that includes all of these flow regions will be a severe test for any viscous computational technique.

Despite the varying streamwise pressure gradient, the laminar velocity profiles near the leading edge on the pressure surface show reasonable agreement with Falkner-Skan velocity profiles (computed at the same streamwise pressure gradient). Transition was identified through a departure of the measured profile shape from the Falkner-Skan profile shape, or through the boundary layer shape factors. Sublimation flow visualization tests agree well with the position of the transition region, but empirical relationships predict onset of transition somewhat early. Transition on the pressure surface was incomplete.

A problem was encountered for the LDV measurements in the extremely thin laminar boundary layers on the pressure surface. Large turbulence intensities were indicated. This problem was traced to a combination of mean-velocity-gradient broadening and measurement volume vibration. Turbulence intensity profiles in the transitional and turbulent boundary layers were not affected.

The leading edge separation "bubble" on the suction surface was too small to be measured. Boundary layers measured downstream of this "bubble" are fully turbulent and the recovery process after reattachment extends downstream a distance of nearly 10% chord. The recovery process can be identified by the velocity profile shapes (including shape factors).

The non-equlibrium turbulent boundary layers downstream of the separation "bubble" follow the wall-wake equation of Coles [1956] until detachment of the boundary layer is reached. These boundary layers also show good similarity using the defect law of Perry and Schofield [1973] up to the location where instantaneous backflow is present. Similarity becomes worse as the amount of instantaneous backflow is increased. No outer region similarity seems to exist downstream of detachment. In the backflow region, however, the data measured here seem to follow the backflow similarity shown by other researchers. Backflow similarity is found by using the maximum backflow velocity as the velocity scale and the total backflow thickness as the length scale.

The near-wake velocity profiles are asymmetric and include negative mean velocities at the wake center. These profiles do not show the Gaussian similarity shown in the far-wake profile measured with a five-hole probe.

Acknowledgments

We would like to extend our appreciation to NASA Lewis for supporting this work (NASA Grant NSG-3264) and to the NASA Lewis personnel for their advice and patience. A special thanks goes to Mr. Nelson Sanger who acted as the grant manager. Professor Robert E. Henderson and Professor Blaine R. Parkin gave valuable support throughout the research project. Other engineering and technical personnel at the Garfield Thomas Water Tunnel were instrumental in the success of the project. Finally, we give a special thanks to the many students who assisted us with the data acquisition and analysis.

X. APPENDIX

Equations for the Double Circular Arc Blades

The equations for the pressure surface, suction surface, and camberline of the double circular arc blades used in the current study can be written as

$$x_p^2 + [y_p + 219.7]^2 = 246.8^2 \quad ,$$

$$x_s^2 + [y_s + 149.5]^2 = 189.1^2 \quad ,$$

and

$$x_c^2 + [y_c + 179.4]^2 = 212.8^2 \quad .$$

All of the dimensions are in millimeters. The origin of the coordinate system used here is located on the chord line of midchord. The x-coordinate is parallel to the chord, while the y-coordinate is normal to the chord.

Nomenclature

AR	aspect ratio
B	integral layer thickness in the Perry and Schofield [1973] theory
c	blade chord length
C	law of the wall constant (= 5.0)
C_f	skin friction coefficient = $\tau_w/(\rho\ U_e^2/2)$
C_p	static pressure coefficient = $(p - p_1)/(\rho\ V_1^2/2)$
D	diffusion factor
H_{12}	first shape factor = δ^*/θ
i	incidence angle = $\beta_1 - \kappa_1$
ID	incipient detachment
ITD	intermittent transitory detachment
L	distance from the surface to the location of τ_{max}
L_p, L_s	pressure and suction surface length scales from the point of maximum velocity to a point where the velocity detect is $(U_e - u_{CL})/2$
LDV	laser Doppler velocimeter
M	Mach number
n	data point index
N	number of data points
p	static pressure
P_T	total or stagnation pressure
r	radius
R_c	radius of curvature
Re_c	blade chord Reynolds number = cV_1/ν
Re_θ	momentum thickness Reynolds number = $\theta U_e/\nu$
s	blade spacing
S_{FV}	location of separation from flow visualization tests

Nomenclature (Cont'd)

TD	transitory detachment
u	streamwise velocity
u'	root mean square value of the turbulent velocity fluctuation
u^+	dimensionless velocity in the inner boundary layer = u/u_τ
u_τ	shear or friction velocity = $\sqrt{\tau_w/\rho}$
U_{BF}	maximum backflow velocity
U_e	velocity at the boundary layer or wake edge
U_m	velocity scale based on the maximum shear stress = $\sqrt{\tau_{max}/\rho}$
U_s	velocity scale for the Perry and Schofield [1973] defect law
V	velocity
W( )	Coles' universal wake function = $2 \sin^2( ) = 1 - \cos( )$
x	streamwise coordinate; blade coordinate (see Appendix)
y	coordinate normal to the blade surface or across the wake; or blade coordinate (see Appendix)
y^+	dimensionless coordinate normal to the blade surface in the inner boundary layer = yu_τ/ν
β	flow angle measured from the axial direction
γ	stagger angle
δ	boundary layer thickness (where $u = 0.99\ U_e$)
δ^*	displacement thickness = $\int_0^\infty \left(1 - \frac{u}{U_e}\right) dy$
δ_{BF}	depth of backflow
δ_D	deviation angle = $\beta_2 - \kappa_2$
ϵ	fluid turning or deflection angle = $\beta_1 - \beta_2$
η	normalized distance across the wake

Nomenclature (Cont'd)

θ	momentum thickness = $\int_0^\infty \frac{u}{U_e}\left(1 - \frac{u}{U_e}\right) dy$
κ	von Karman's mixing length parameter (= 0.41); blade metal angle
ν	kinematic viscosity (0.150 cm^2/sec for air)
Π	Coles' wake parameter
ρ	fluid density (1.205 kg/m^3 for air)
σ	blade solidity = c/s
τ_{max}	maximum shear stress
τ_w	wall or surface shear stress
ϕ	camber angle = $\kappa_1 - \kappa_2$
ω	total-pressure loss coefficient = $(P_{T_1} - P_{T_2})/(\rho\ V_1^2/2)$

Subscripts

c	camber line
CL	at the wake centerline
inv	inviscid
LE	leading edge
m	mean flow
meas	measured
n	data point index
p	pressure surface
s	suction surface
TE	trailing edge
x	axial direction
θ	tangential direction

Nomenclature (Cont'd)

1	inlet (upstream five-hole probe measurement station)
2	outlet (downstream five-hole probe measurement station)

Superscript

$\overline{\quad}$	average over the blade passage

IX. REFERENCES

1. Abu-Ghannam, B. J. and Shaw, R., "Natural Transition of Boundary Layers--The Effects of Turbulence, Pressure Gradient, and Flow History," Journal of Mechanical Engineering Science, Vol. 22, No. 5, pp. 213-228, 1980.

2. Anand, A. K. and Lakshminarayana, B., "An Experimental Study of Three-Dimensional Turbulent Boundary Layer and Turbulence Characteristics Inside a Turbomachinery Rotor Passage," Transactions of the ASME, Journal of Engineering for Power, Vol. 100, pp 676-690, October 1978.

3. Ball, C. L., Reid, L., and Schmidt, J. F., "End-Wall Boundary Layer Measurements in a Two Stage Fan," NASA TM 83409, June 1983.

4. Bammert, K. and Milsch, R., "Boundary Layers on Rough Compressor Blades," ASME Paper No. 72-GT-48, 1972.

5. Bammert, K. and Sandstede, H., "Measurements of the Boundary Layer Development along a Turbine Blade with Rough Surfaces," Transactions of the ASME, Journal of Engineering for Power, Vol. 102, pp 978-983, October 1980.

6. Beam, R. M. and Warming, R. F., "An Implicit Factored Scheme for the Compressible Navier-Stokes Equations," AIAA Journal, Vol. 16, No. 4, pp. 393-402, April 1982.

7. Braden, J. A., Whipkey, R. R., Jones, G. S., and Lilley, D. E., "Experimental Study of the Separating Confluent Boundary-Layer," NASA Contractor Report 3655, June 1983.

8. Bradshaw, P., Ferriss, D. H., and Atwell, W. P., "Calculation of Boundary Layer Development Using the Turbulent Energy Equation," Journal of Fluid Mechanics, Vol. 28, pp. 593-616, 1967.

9. Bradshaw, P., "The Analogy Between Streamline Curvature and Buoyancy in Turbulent Shear Flow," Journal of Fluid Mechanics, Vol. 26, pp. 177-191, 1969.

10. Briley, W. R. and McDonald, H., "Three-Dimensional Viscous Flows With Large Secondary Velocity," Journal of Fluid Mechanics, Vol. 144, pp. 47-77, July 1984.

11. Clauser, F. H., "Turbulent Boundary Layers in Adverse Pressure Gradients," Journal of the Aeronautical Sciences, Vol. 21, pp. 91-108, February 1954.

12. Coles, D. E., "The Law of the Wake in the Turbulent Boundary Layer," Advances in Applied Mechanics, Vol. 1, pp. 191-226, 1956.

13. Davis, R. T. and Werle, M. J., "Progress on Interacting Boundary-Layer Computations at High Reynolds Number," Numerical and Physical Aspects of Aerodynamic Flows, Edited by T. Cebeci, Springer-Verlag, 1981.

14. Edwards, D. E. and Carter, J. E., "A Quasi-Simultaneous Finite Difference Approach for Strongly Interacting Flow," Presented at the Third Symposium on Numerical and Physical Aspects of Aerodynamic Flows, January 21-29, 1985.

15. Edwards, R. V., Angus, J. C., French, M. J., and Dunning, J. W., Jr., "Spectral Analysis of the Signal From the Laser Doppler Flowmeter: Time-Dependent Systems," Journal of Applied Physics, Vol. 42, No. 3, pp. 837-850, February 1971.

16. Edwards, R. V., "A New Look at Particle Statistics in Laser-Anemometer Measurements," Journal of Fluid Mechanics, Vol. 105, pp. 317-325, 1981.

17. Edwards, R. V. and Jensen, A. S., "Particle-Sampling Statistics in Laser Anemometers: Sample-and-Hold Systems and Saturbale Systems," Journal of Fluid Mechanics, Vol. 133, pp. 397-411, 1983.

18. Evans, B. J., "Effects of Free-Stream Turbulence on Blade Performance in a Compressor Cascade," Ph.D. Dissertation, Cambridge University, 1971.

19. Evans, R. L., "Boundary Layer Development on an Axial-Flow Compressor Stator Blade," Transactions of the ASME, Journal of Engineering for Power, Vol. 100, pp. 287-293, April 1978.

20. Falkner, V. M. and Skan, S. W., "Some Approximate Solutions of the Boundary Layer Equations," Phil. Mag., Vol. 12, No. 7, pp.865-896, 1931.

21. Gibson, M. M., Verriopoulos, C. A., and Vlachos, N. S., "Turbulent Boundary Layer on a Mildly Curved Convex Surface--Part 1: Mean Flow and Turbulence Measurements," Experiments in Fluids, Vol. 2, pp. 17-24, 1984.

22. Giel, T. V. and Barnett, D. O., "Analytical and Experimental Study of Statistical Bias in Laser Velocimetry," Laser Velocimetry and Particle Sizing, Edited by H. D. Thompson and W. H. Stevenson, Hemisphere Publishing Corporation, pp. 86-99, 1979.

23. Gillis, J. C. and Johnston, J. P., "Turbulent Boundary-Layer Flow and Structure on a Convex Wall and Its Redevelopment on a Flat Wall," Journal of Fluid Mechanics, Vol. 135, pp. 123-153, 1983.

24. Goldstein, R. J. and Adrian, R. J., "Measurement of Fluid Velocity Gradients Using Laser-Doppler Techniques," The Review of Scientific Instruments, Vol. 42, No. 9, pp. 1312-1320, September 1971.

25. Görtler, H., "Über eine dreidimensionale Instabilität laminarer Grenzschichten an konkaven Wänden," Nachr. Ges. Wiss. Göttingen, Math. Phys. Klasse, New series 2, No. 1, 1940.

26. Hah, C. and Lakshminarayana, B., "Measurement and Prediction of Mean Velocity and Turbulence Structure in the Near Wake of an Airfoil," Journal of Fluid Mechanics, Vol. 115, pp. 251-282, 1982.

27. Hobbs, D. E., Wagner, J. H., Dannenhoffer, J. F., and Dring, R. P., "Experimental Investigation of Compressor Cascade Wakes," ASME Paper No. 82-GT-299, 1982.

28. Hodson, H. P., "The Development of Unsteady Boundary Layers on the Rotor on an Axial-Flow Turbine," AGARD-CP-351, June 1983.

29. Hoesel, W. and Rodi, W., "New Biasing Elimination Method for Laser-Doppler Velocimeter Counter Processing," Review of Scientific Instrumentation, Vol. 48, No. 2, July 1977.

30. Holmes, B. J. and Obara, C. J., "Observations and Implications of Natural Laminar Flow on Practical Airplane Surfaces," Thirteenth Congress of ICAS and AIAA, Aircraft Systems and Technology Conference, Seattle, Washington, ICAS-82-5.1.1, August 22-27, 1982.

31. Johnson, D. A., Modarress, D., and Owen, F. K., "An Experimental Verification of Laser-Velocimeter Sampling Bias and Its Correction," Transactions of the ASME, Journal of Fluids Engineering, Vol. 106, pp. 5-12, March 1984.

32. Johnston, W. and Sockol, P., "Viscous-Inviscid Interactive Procedure for Rotational Flow in Cascades of Airfoils," AIAA Journal, Vol. 22, No. 9, pp. 1281-1282, September 1984.

33. Klebanoff, P. S., Tidstrom, K. D., and Sargent, L. M., "The Three-Dimensional Nature of Boundary-Layer Instability," Journal of Fluid Mechanics, Vol. 12, No. 1, pp. 1-34, 1962.

34. Kreid, D. K., "Laser-Doppler Velocimeter Measurements in Nonuniform Flow: Error Estimates," Applied Optics, Vol. 13, No. 8, pp. 1872-1881, August 1974.

35. Lakshminarayana, B. and Davino, R., "Mean Velocity and Decay Characteristics of the GuideVane and Stator Blade Wake of an Axial Flow Compressor," Transactions of the ASME, Journal of Engineering for Power, Vol. 102, pp. 50-60, January 1980.

36. Lakshminarayana, B., Govindan, T. R., and Hah, C., "Experimental Study of the Boundary Layer on a Turbomachine Rotor Blade," In Three-Dimensional Turbulent Boundary Layers, IUTAM Symposium, Berlin, March 29-April 1, 1982.

37. Launder, B. E., Reece, G. J., and Rodi, W., "Progress in the Development of a Reynolds Stress Turbulence Closure," Journal of Fluids Mechanics, Vol. 68, pp. 537-566, 1975.

38. Lieblein, S. and Roudebush, W. H., "Theoretical Loss Relations for Low-Speed Two-Dimensional-Cascade Flow," NACA TN 3662, 1956.

39. Lieblein, S., Schwenk, F. C., and Broderick, R. L., "Diffusion Factor for Estimating Losses and Limiting Blade Loadings in Axial-Flow-Compressor Blade Elements," NACA RM E53D01, June 8, 1953.

40. Ludweig, H. and Tillman, W., "Untersuchungen über die Wandschubspannung in Turbulenten Reibungsschenhten," Ing.-Arch., Vol. 17, pp. 288-299, 1949.

41. McLaughlin, D. K. and Tiederman, W. G., "Biasing Correction for Individual Realization of Laser Anemometer Measurements in Turbulent Flows," Physics of Fluids, Vol. 16, No. 12, pp. 2082-2088, December 1973.

42. Meauzé, G., "Transonic Boundary Layer on Compressor Stator Blades as Calculated and Measured in Wind Tunnel," At the Fourth International Symposium on Air Breathing Engines--ISABE, April 1-6, 1979.

43. Mehta, J. M. and Goradia, S., "Experimental Studies of the Separated Flow Over a NASA GA(W)-1 Airfoil," AAIA Journal, Vol. 22, No. 4, pp. 552-554, April 1984.

44. Mellor, G. L. and Gibson, D. M., "Equilibrium Turbulent Boundary Layers," Journal of Fluid Mechanics, Vol. 24, Part 2, pp. 225-253, 1966.

45. Mellor, G. L. and Wood, G. M., "An Axial Compressor End-Wall Boundary Layer Theory," Transactions of the ASME, Journal of Basic Engineering, Vol. 93, Series D, No. 1, pp. 300-316, June 1971.

46. Melnik, R. E. and Brook, J. W., "The Computation of Viscid/Inviscid Interaction on Airfoils With Separated Flow," Gruman Aerospace Corporation Report RE-697, April 1985.

47. Murlis, J., Tsai, H. M., and Bradshaw, P., "The Structure of Turbulent Boundary Layers at Low Reynolds Numbers," Journal of Fluid Mechanics, Vol. 122, pp. 13-56, 1982.

48. Perry, A. E. and Schofield, W. H., "Mean Velocity and Shear Stress Distributions in Turbulent Boundary Layers," Physics of Fluids, Vol. 16, No. 12, pp. 2068-2074, December 1973.

49. Peterson, C. R., "Boundary Layer on an Airfoil in a Cascade," Gas Turbine Laboratory Report No. 49, Massachusetts Institute of Technology, December 1958.

50. Pollard, D. and Gostelow, J. P., "Some Experiments at Low Speed on Compressor Cascades," Transactions of the ASME, Journal of Engineering for Power, Vol. 89, Series A, pp. 427-436, June 1967.

51. Pouagare, M., Galmes, J. M., and Lakshminarayana, B., "An Experimental Study of the Compressor Rotor Blade Boundary Layer," Transactions of the ASME, Journal of Engineering for Gas Turbines and Power, Vol. 107, pp. 364-373, April 1985.

52. Purtell, L. R., Klebanoff, P. S., and Buckley, F. T., "Turbulent Boundary Layers at Low Reynolds Numbers," Physics of Fluids, Vol. 24, pp. 802-811, 1982.

53. Ramaprian, B. R. and Shivaprasad, B. G., "Mean Flow Measurements in Turbulent Boundary Layers Along Mildly Curved Surfaces," AIAA Journal, Vol. 15, No. 2, pp. 189-196, February 1977.

54. Rubin, S. G. and Khosla, P. K., "Navier-Stokes Calculations With a Coupled Strongly Implicit Method. Part I--Finite Difference Solutions," Computers and Fluids, Vol. 9, No. 2, p. 163, 1981.

55. Rubin, S. G. and Khosla, P. K., "A Composite Velocity Procedure for the Incompressible Navier-Stokes Equations," 8th International Conference on Numerical Methods in Fluid Mechanics, Springer-Verlag, pp. 448-454, 1982.

56. Sandborn, V. A. and Kline, S. J., "Flow Models in Boundary Layer Stall Inception," Transactions of the ASME, Journal of Basic Engineering, Vol. 83, pp. 317-327, May 1961.

57. Sanger, N., Double Circular Arc Compressor Blades, NASA Lewis DCA4, 65 Degree Camber Centerline and Thickness Equations, Private Communication, November 1980.

58. Schofield, W. H., "Equilibrium Boundary Layers in Moderate to Strong Adverse Pressure Gradients," Journal of Fluid Mechanics, Vol. 113, pp. 91-122, 1981.

59. Schofield, W. H., "On Separating Turbulent Boundary Layers," Mechanical Engineering Report 162, Department of Defense, Defense Science and Technology Organization, Aeronautical Research Laboratories, September 1983.

60. Shivaprasad, B. G. and Ramaprian, B. R., "Turbulence Measurements in Boundary Layers Along Mildly Curved Surfaces," Transactions of the ASME, Journal of Fluids Engineering, Vol. 100, pp. 37-46, March 1978.

61. Simpson, R. L., Strickland, J. H., and Barr, P. W., "Features of a Separating Turbulent Boundary Layer in the Vicinity of Separation," Journal of Fluid Mechanics, Vol. 79, Part 3, pp. 553-594, 1977.

62. Simpson, R. L., Chew, Y.-T., and Shivaprasad, B. G., "The Structure of a Separating Turbulent Boundary Layer. Part 1. Mean Flow and Reynolds Stresses," Journal of Fluid Mechanics, Vol. 113, pp. 23-51, 1981.

63. Smits, A. J., Matheson, N., and Joubert, P. N., "Low-Reynolds-Number Turbulent Boundary Layers in Zero and Favorable Pressure Gradients," Journal of Ship Research, Vol. 27, No. 3, pp. 147-157, September 1983.

64. So, R. M. C. and Mellor, G. L., "Experiment on Convex Curvature Effects in Turbulent Boundary Layers," Journal of Fluid Mechanics, Vol. 60, pp. 43-62, 1973.

65. So, R. M. C., "A Turbulence Velocity Scale For Curved Shear Flows," Journal of Fluid Mechanics, Vol. 70, Part 1, pp. 37-57, 1975.

66. Steger, J. L., "Implicit Finite-Difference Simulation of Flow About Arbitrary Two-Dimensional Geometries," AIAA Journal, Vol. 16, pp. 679-686, 1978.

67. Stevenson, W. H., Thompson, H. D., and Craig, R. R., "Laser Velocimeter Measurements in Highly Turbulent Recirculating Flows," Transactions of the ASME, Journal of Fluids Engineering, Vol. 106, pp. 173-180, June 1984.

68. Thompson, J., "Numerical Solution of Flow Problems Using Body-Fitted Coordinate Systems," in Computational Fluid Dynamics, Lecture at von Karman Institute, edited by W. Kollmann, Hemisphere Publication, New York, NY, p. 1. 1980.

69. Toyokura, T., Kurokawa, J., and Kimoto, Y., "Three-Dimensional Boundary Layer Flow on Rotating Blades," Transactions of the JSME, Vol. 25, 1982.

70. Treaster, A. L. and Yocum, A. M., "The Calibration and Application of Five-hole Probes," Transactions of the Instrument Society of America, Vol. 18, No. 3, pp. 23-34, 1979.

71. Wadcock, A. J., "Simple Turbulence Models and Their Application to Boundary Layer Separation," NASA Contractor Report 3283, May 1980.

72. Walker, G. J., "The Turbulent Boundary Layer on an Axial Compressor Blade," ASME Paper No. 82-GT-52, 1982.

73. Wang, T., Simon, T. W., and Buddhavarapu, J., "Heat Transfer and Fluid Mechanics Measurements in Transitional Boundary Layer Flows," ASME Paper No. 85-GT-113, 1985.

74. Wills, J. A. B., "Correction of Hot Wire Readings for Proximity to a Solid Boundary," Journal of Fluid Mechanics, Vol. 12, pp. 388-396, 1962.

75. Zierke, W. C. and Deutsch, S., "An Analysis to Facilitate the Interpretation of Boundary Layer Measurements," ARL/PSU TM 85-85, The Applied Research Laboratory, The Pennsylvania State University, May 25, 1985.

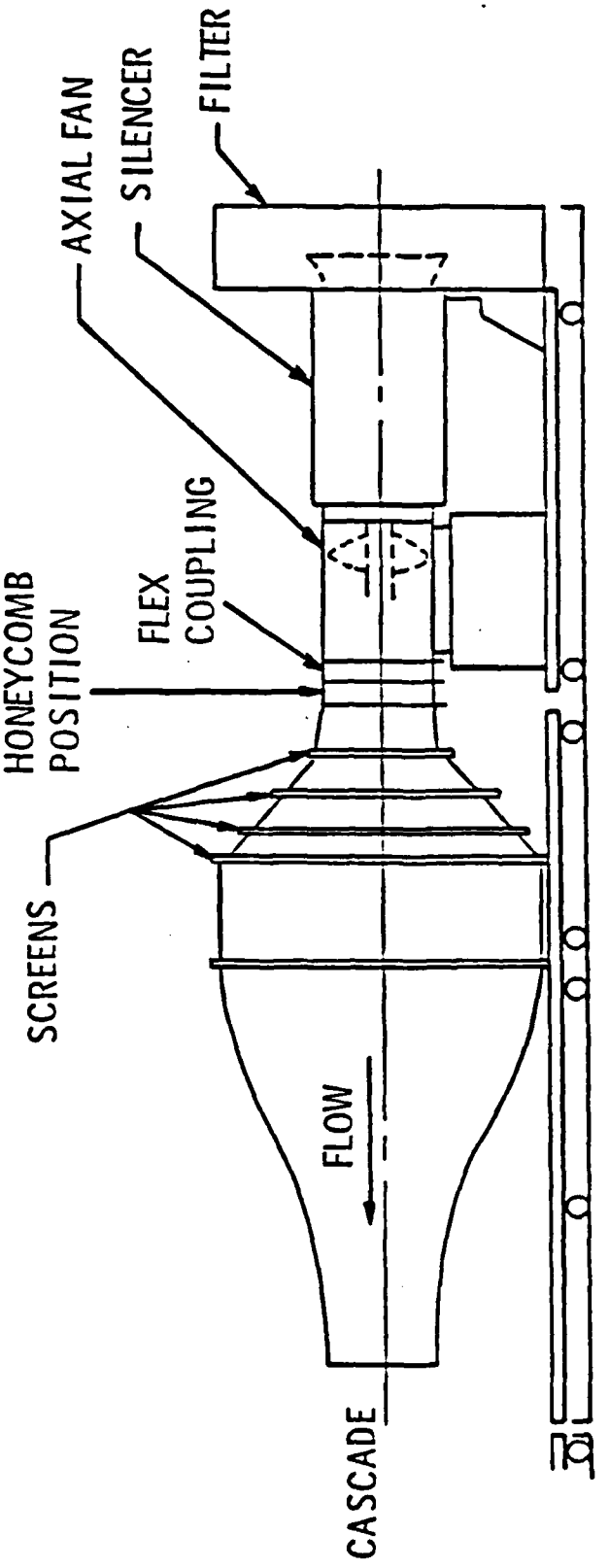

Figure 1. Open Return Wind Tunnel

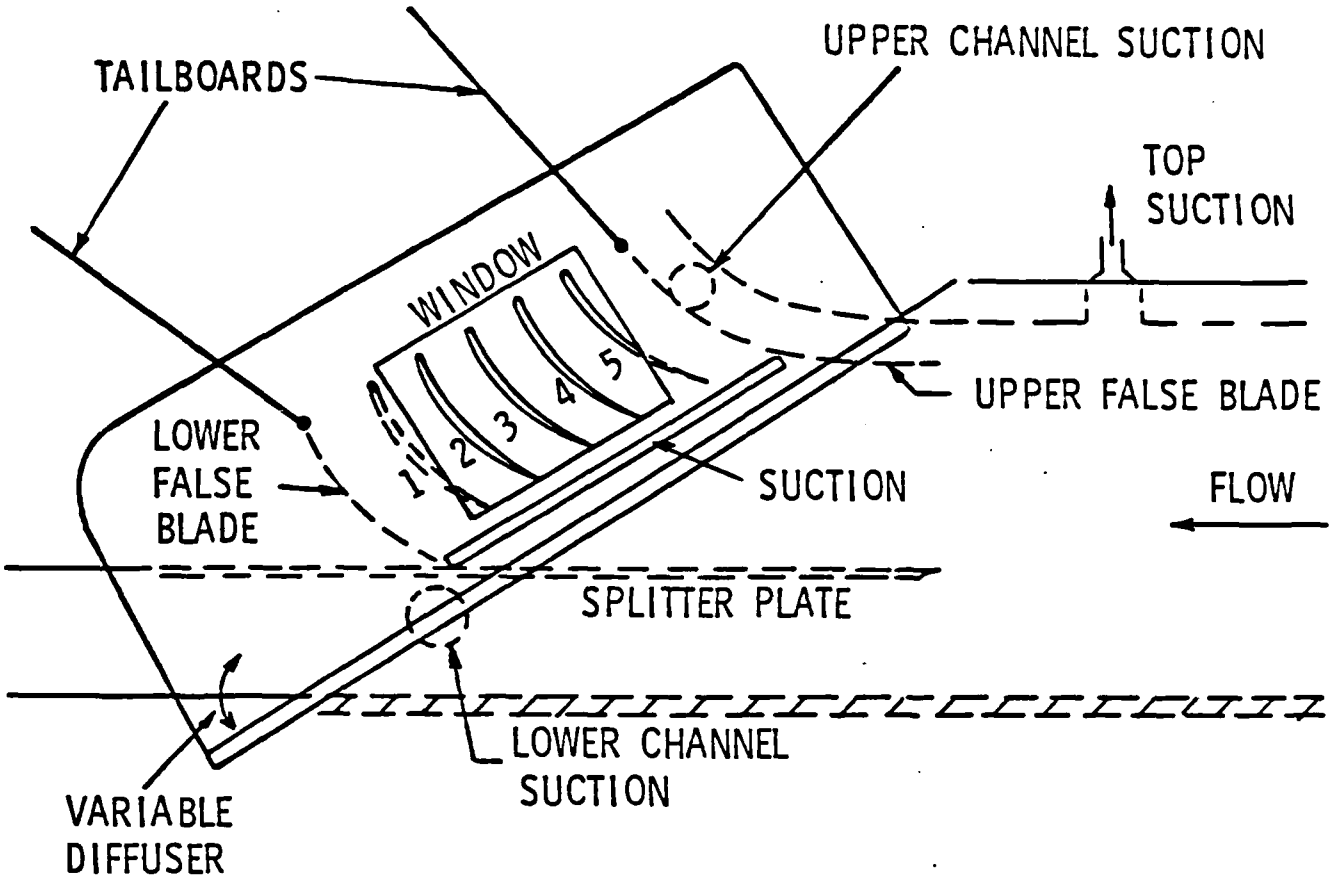

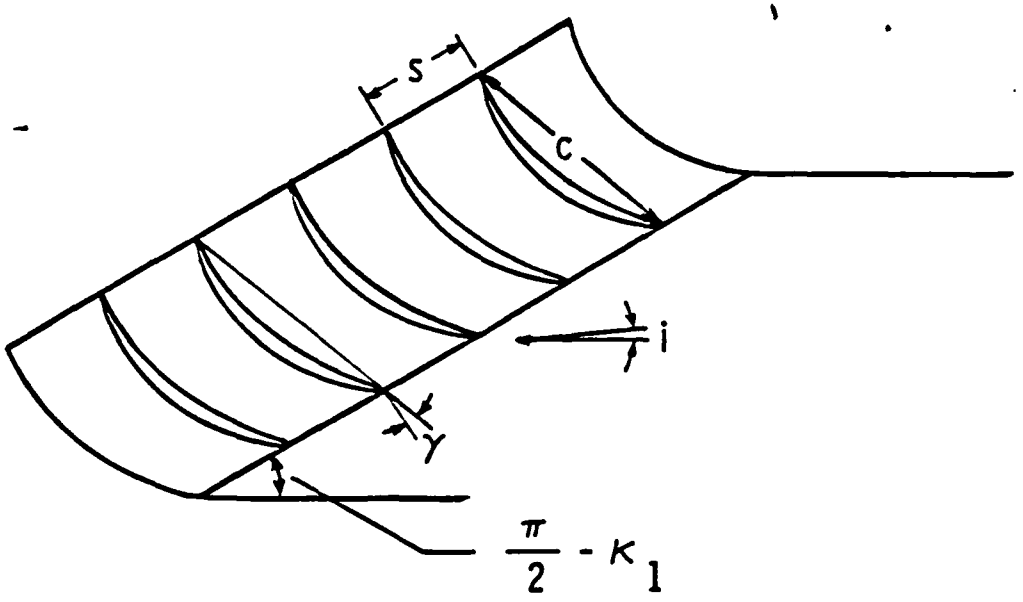

Figure 2. Cascade Test Section with Flow Controls

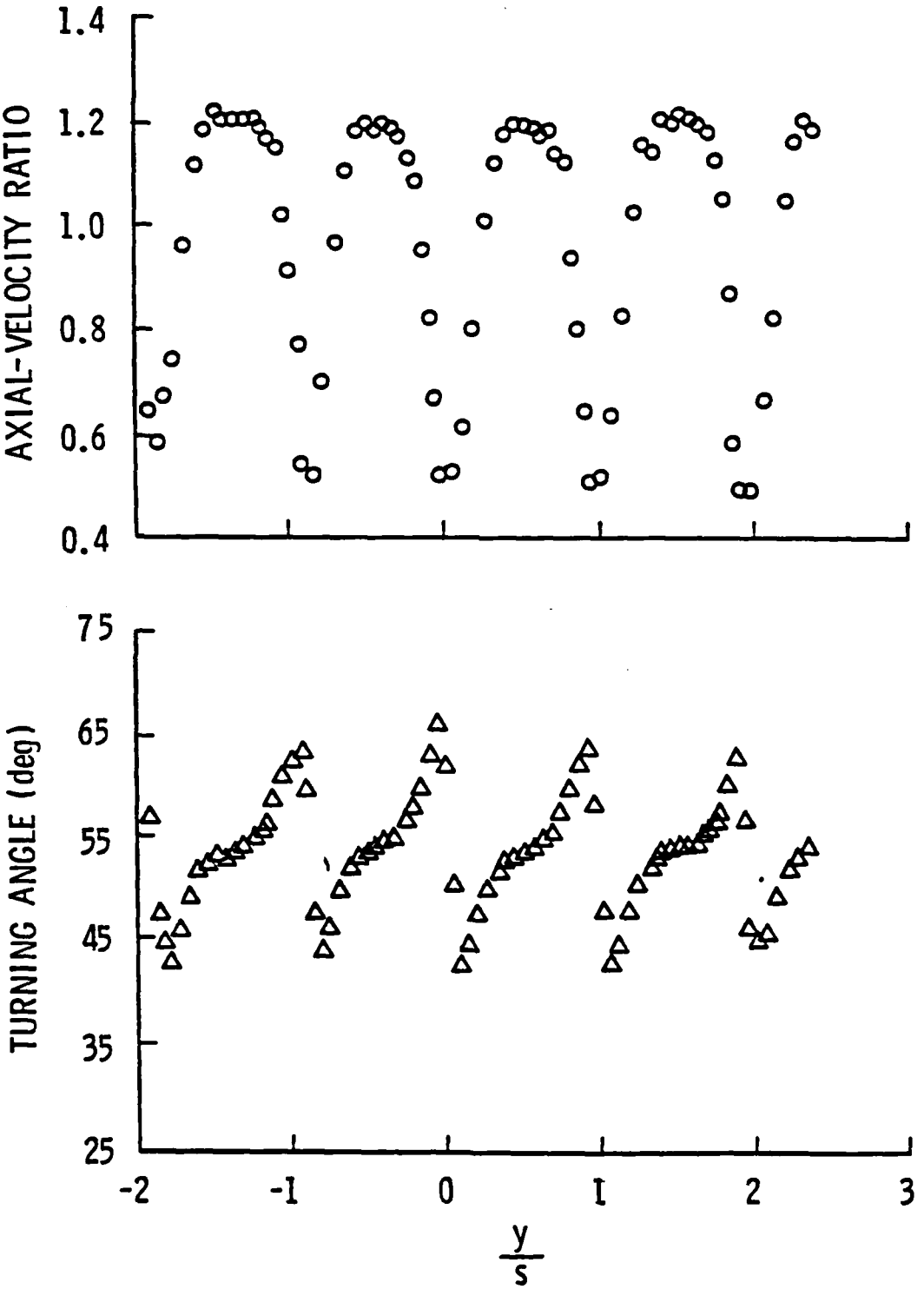

Figure 3. Five-Hole Probe Outlet Survey

BLADE GEOMETRY

$C = 228.6$ mm	$\sigma = 2.14$	$\kappa_1 = 53^0$
$S = 106.8$ mm	$AR = 1.61$	$\kappa_2 = -12^0$
$r_{LE} = r_{TE} = 9.14\ \mu m$	$\gamma = 20.5^0$	$\phi = 65^0$

MEASURED FLOW CONDITIONS

$Re_c \approx 500,000$	$V_X = 17.55$ m/sec	$\overline{\beta}_m = 39.9^0$
$i = 5^0$	$\overline{\beta}_2 = 4^0$	$\overline{\theta} = 54^0$
$\beta_1 = 58^0$	$\overline{V}_2 = 17.59$ m/sec	$\overline{\delta}_D = 16^0$
$V_1 = 33.11$ m/sec	$\overline{V}_m = 22.88$ m/sec	$\overline{\omega} = 0.151$
		$\left(\overline{C_p}\right)_2 = 0.463$

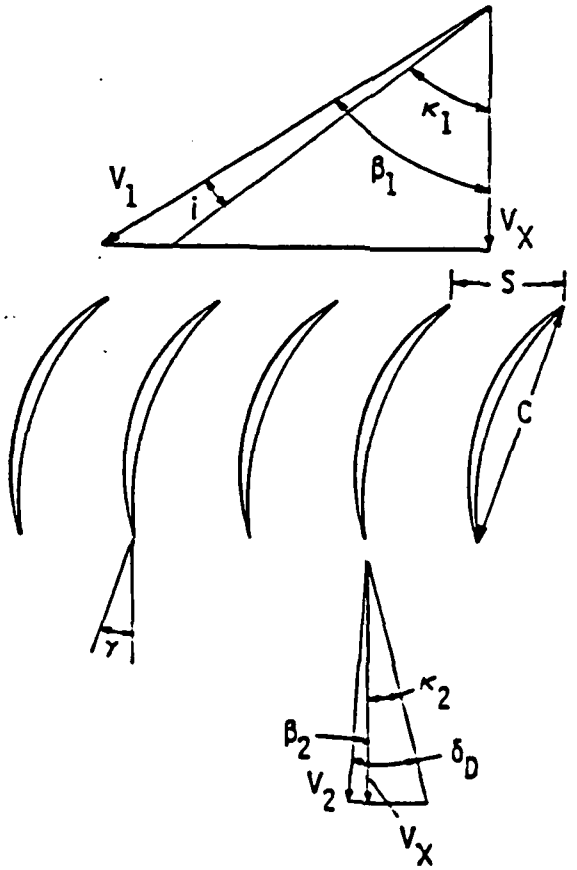

Figure 4. Blade Geometry and Flow Conditions

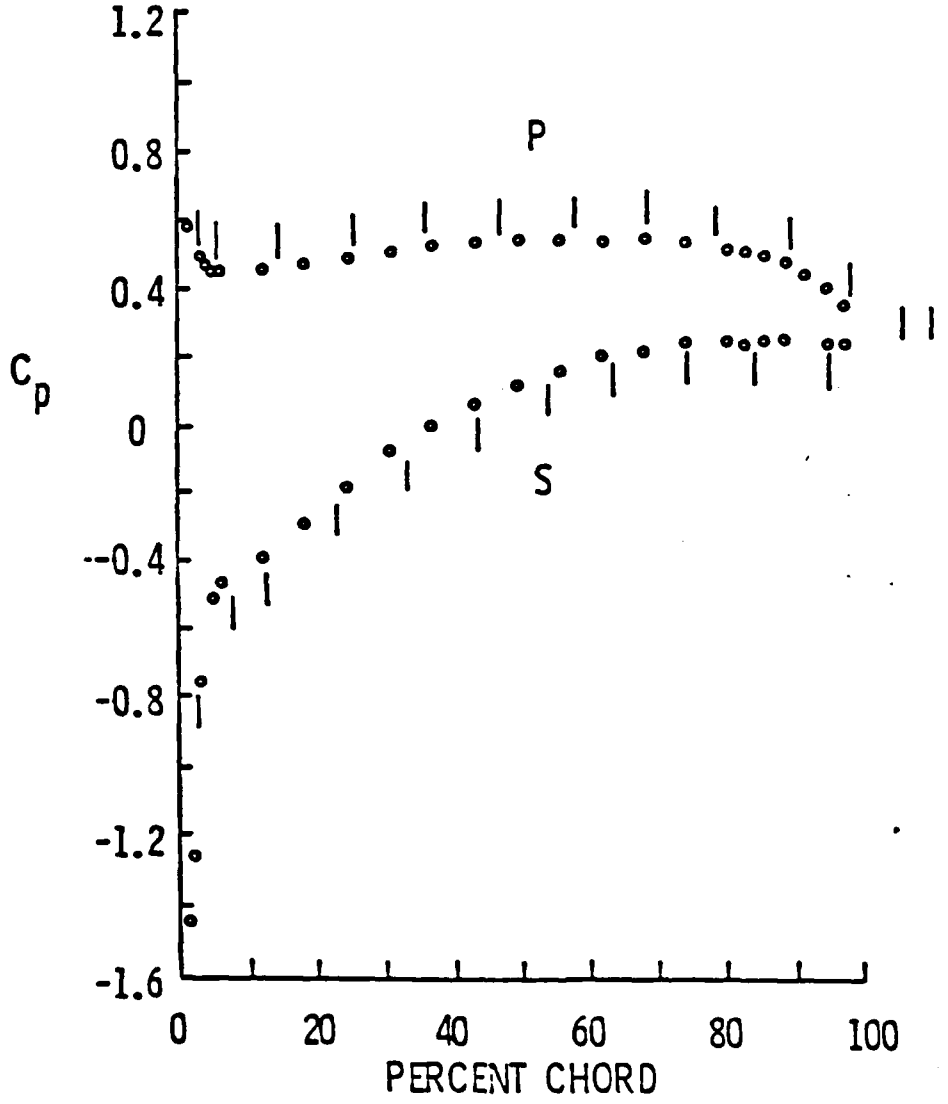

Figure 5. Blade Static-Pressure Distribution (The Vertical Line Segments Represent the Locations of LDV Measurements) (P - Pressure Surface; S - Suction Surface)

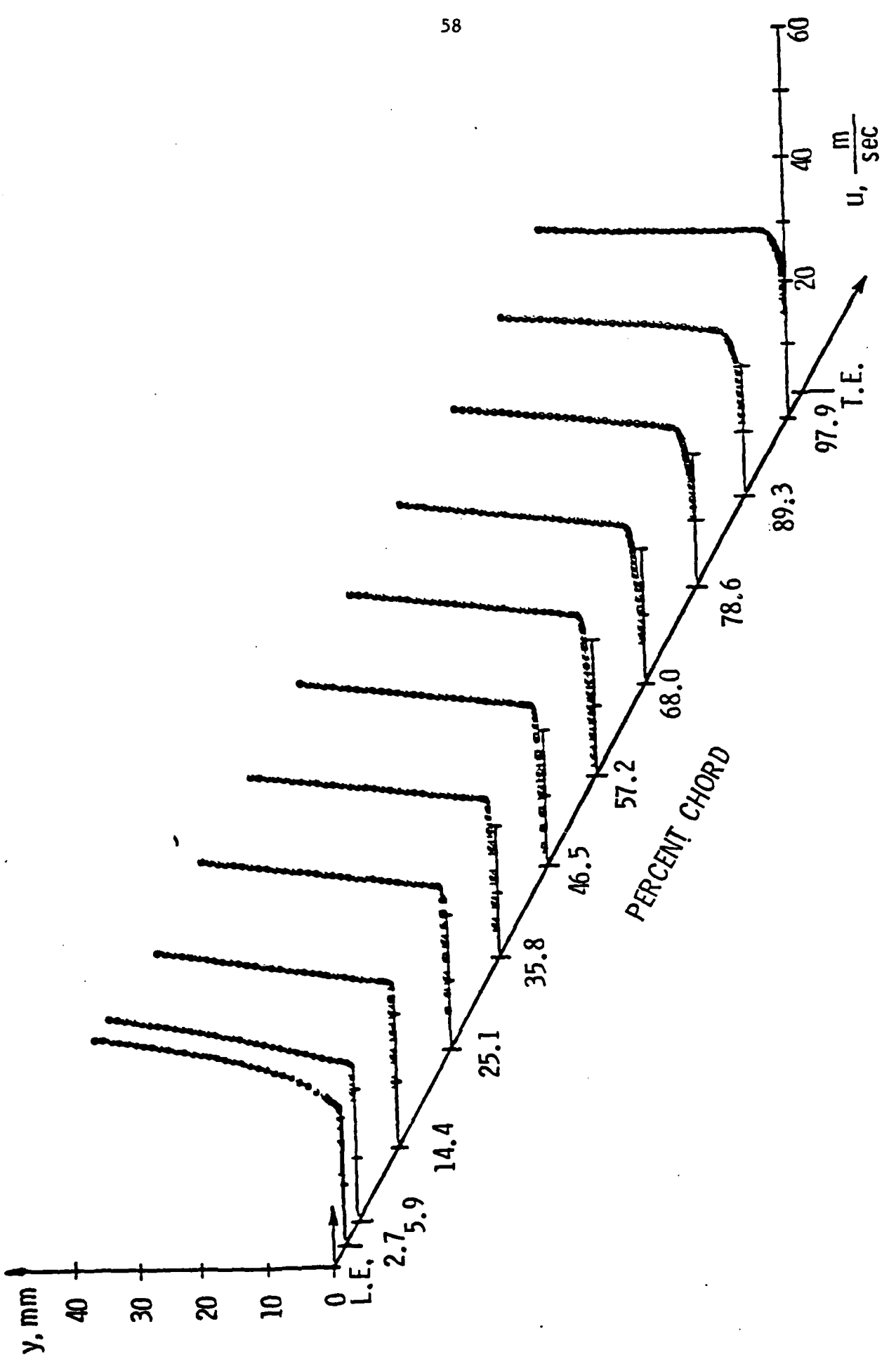

Figure 6. Measured Pressure Surface Boundary Layers

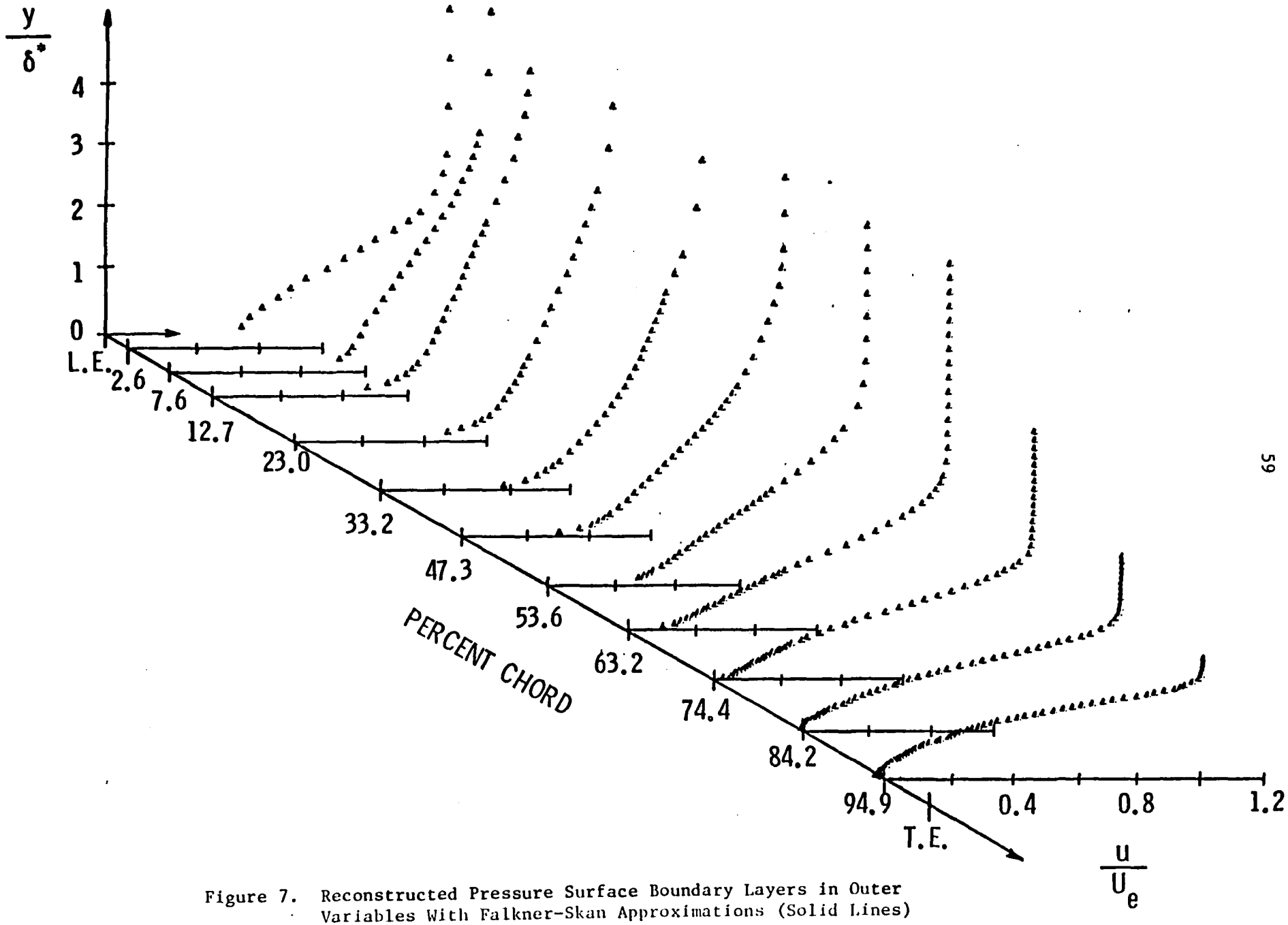

Figure 7. Reconstructed Pressure Surface Boundary Layers in Outer Variables With Falkner-Skan Approximations (Solid Lines)

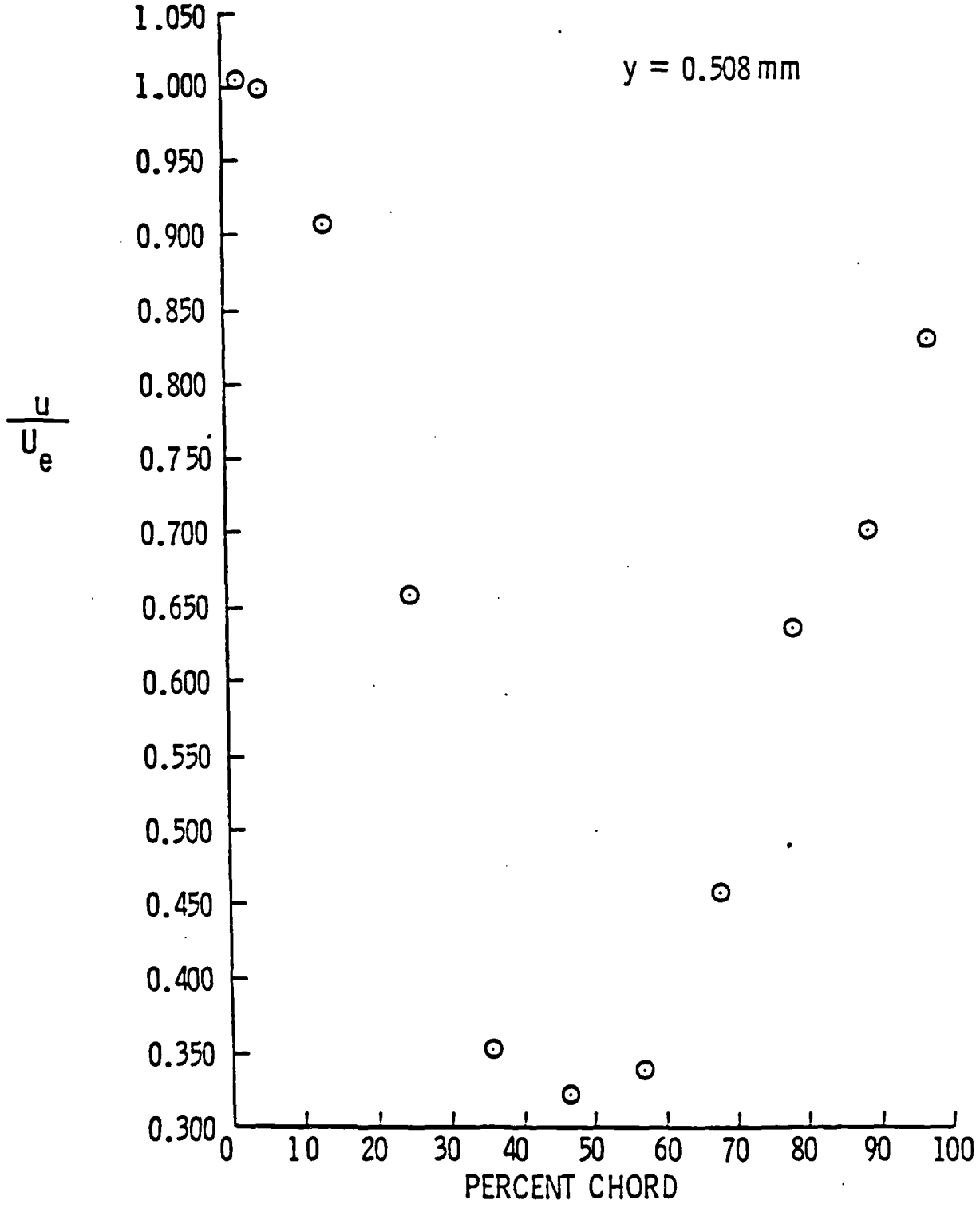

Figure 8. Variation of Velocity, 0.508 mm From the Blade, on the Pressure Surface

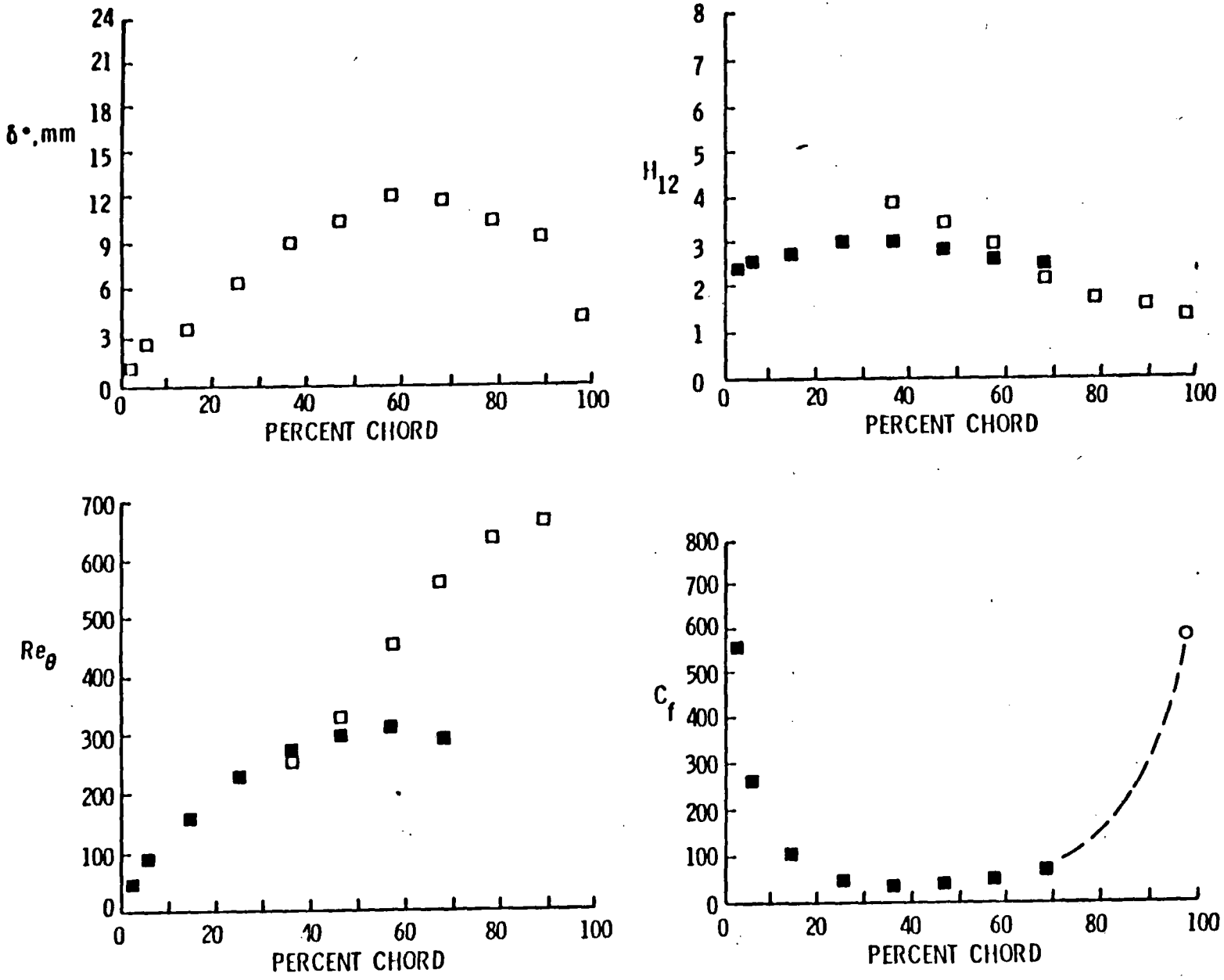

Figure 9. Variation of Displacement Thickness, First Shape Factor, Momentum Thickness Reynolds Number, and Skin Friction Coefficient on the Pressure Surface (- Obtained from a Smoothed Cubic Spline Fit; - Obtained from a Falkner Skan Approximation, - Obtained From a Smoothed Cubic Spline Fit and Ludweig-Tillman Equation)

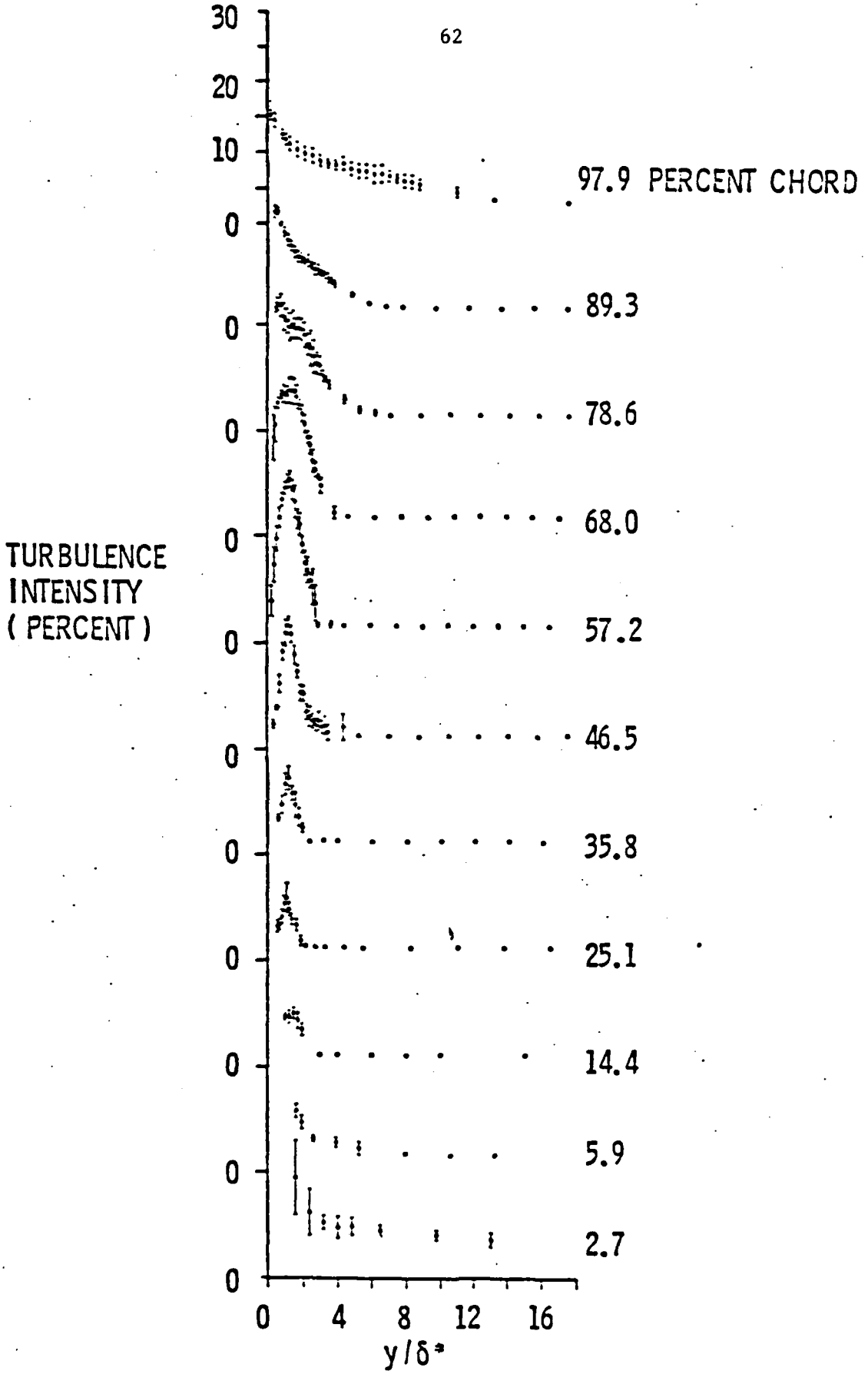

Figure 10. Turbulence Intensity Data for the Pressure Surface Boundary Layers

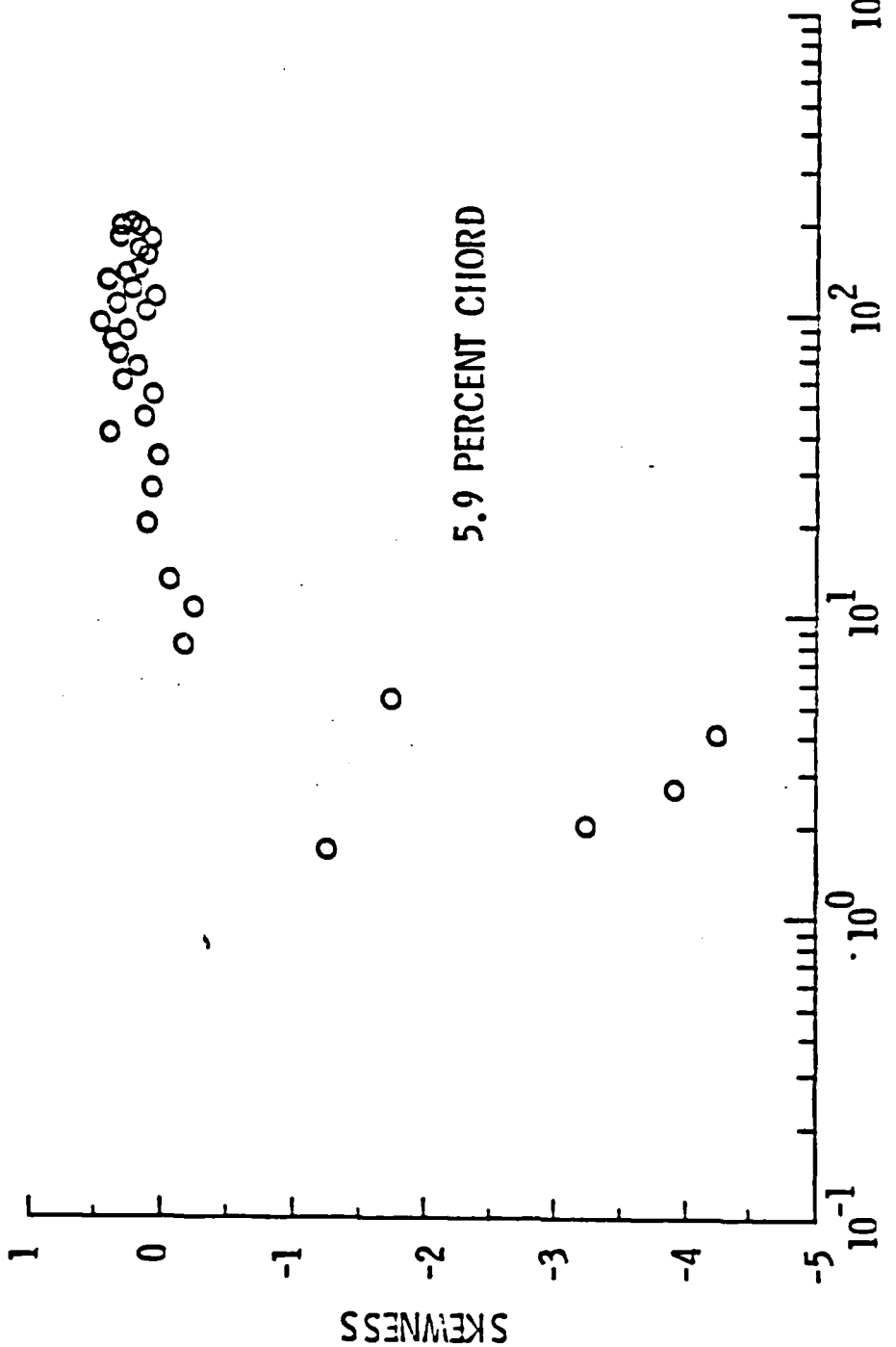

Figure 11. Skewness Distribution for the Pressure Surface Boundary Layer at 5.9% Chord

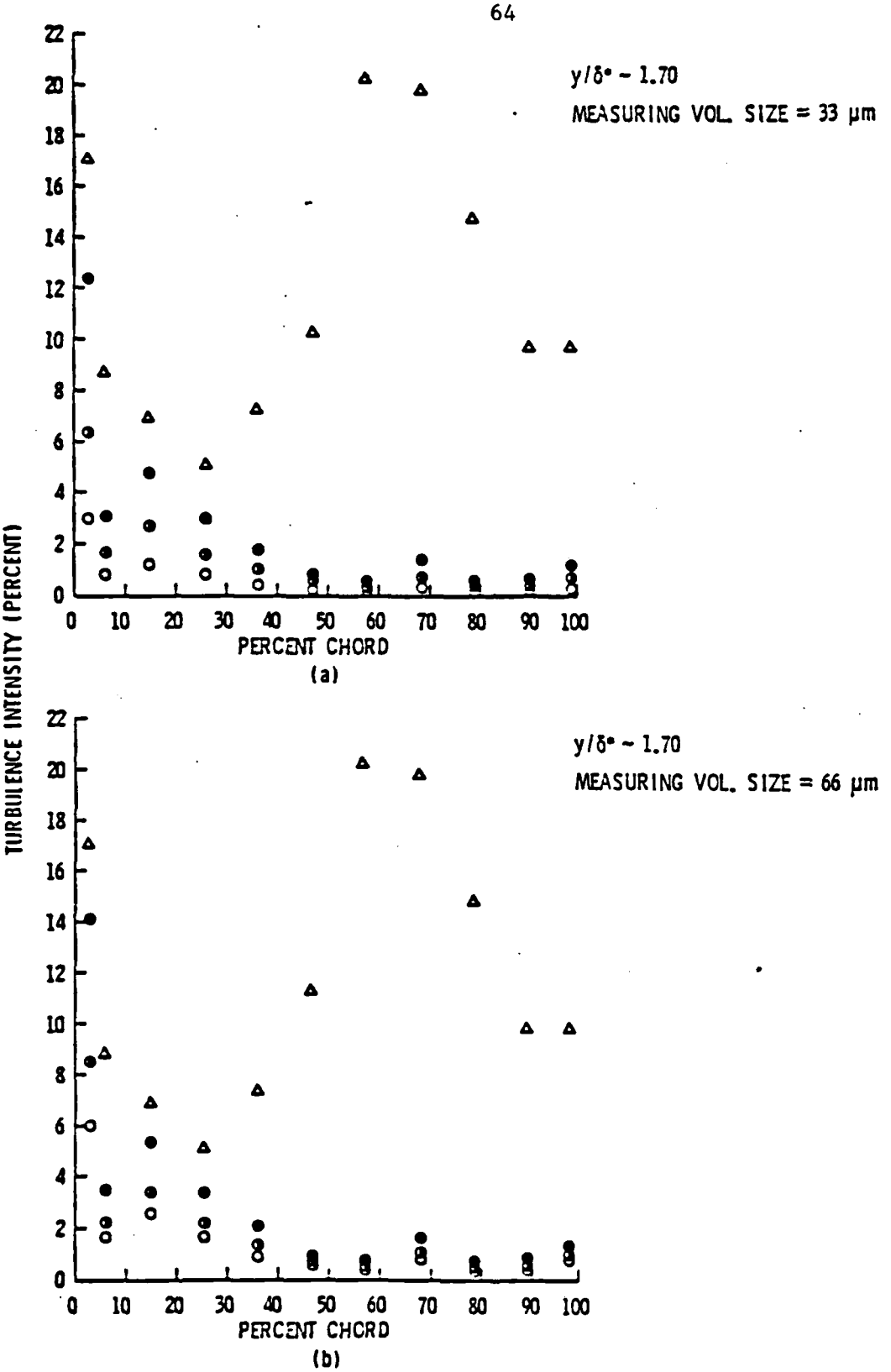

Figure 12. Pressure Surface Turbulence Intensities at $y/\delta^* \sim 1.70$, Both Measured Data and Data Estimated by Mean-Velocity-Gradient Broadening and Measurement Volume Vibration (- Measured Data; - Vibration Amplitude of 0 μm; - Vibration Amplitude of 25.4 μm; Vibration Amplitude of 50.8 μm)

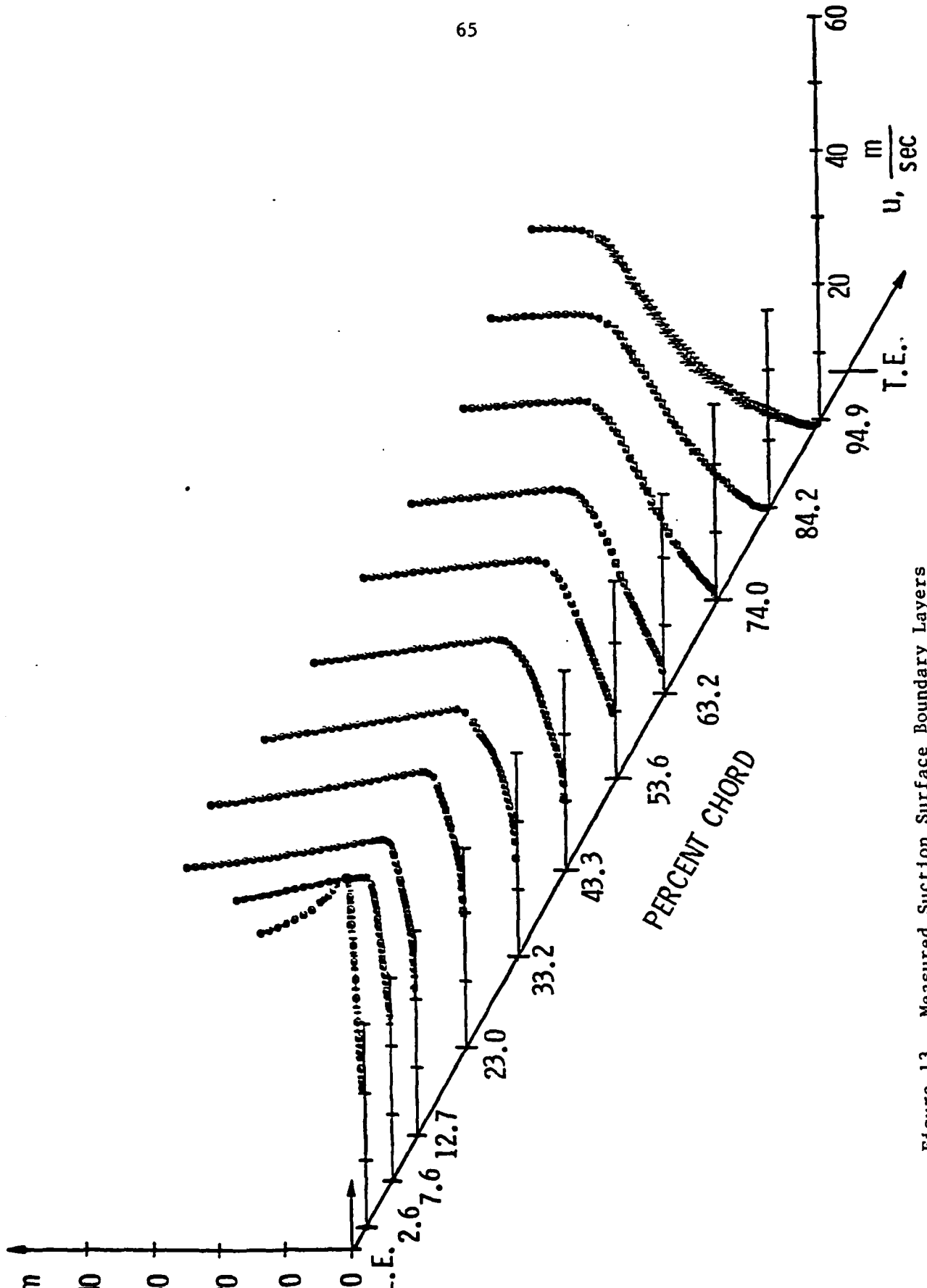

Figure 13. Measured Suction Surface Boundary Layers

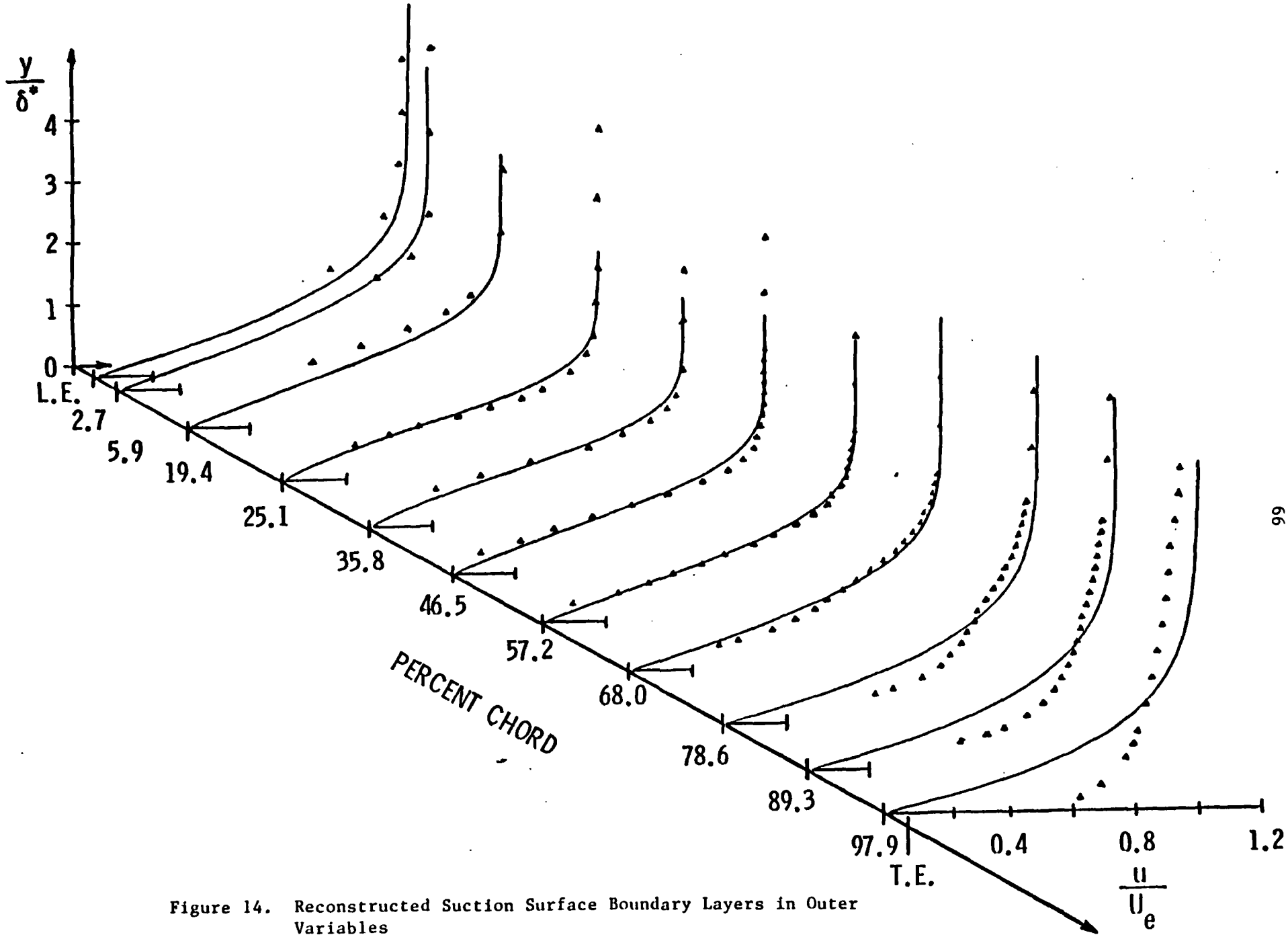

Figure 14. Reconstructed Suction Surface Boundary Layers in Outer Variables

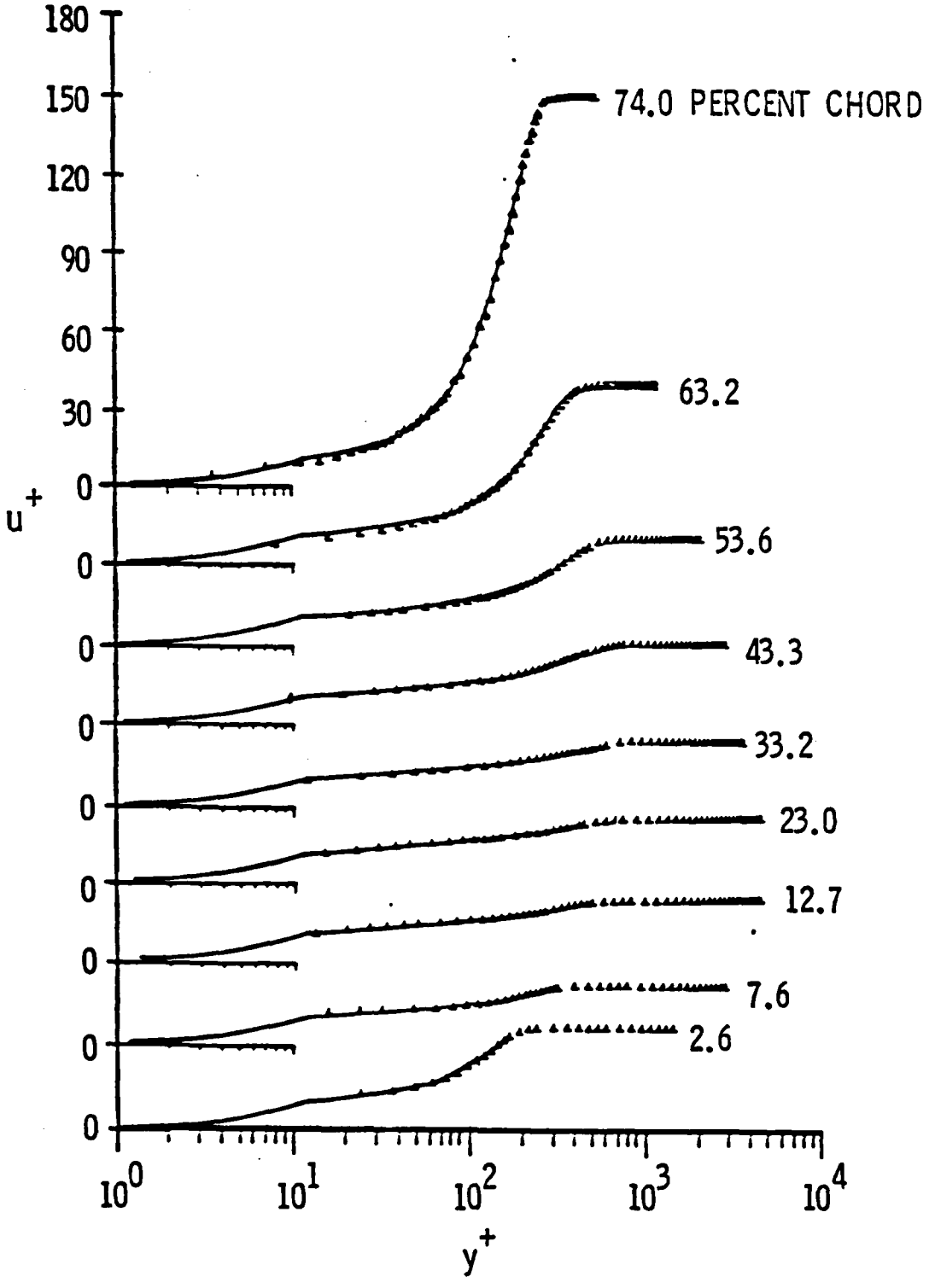

Figure 15. Reconstructed Suction Surface Boundary Layers in Inner Variables

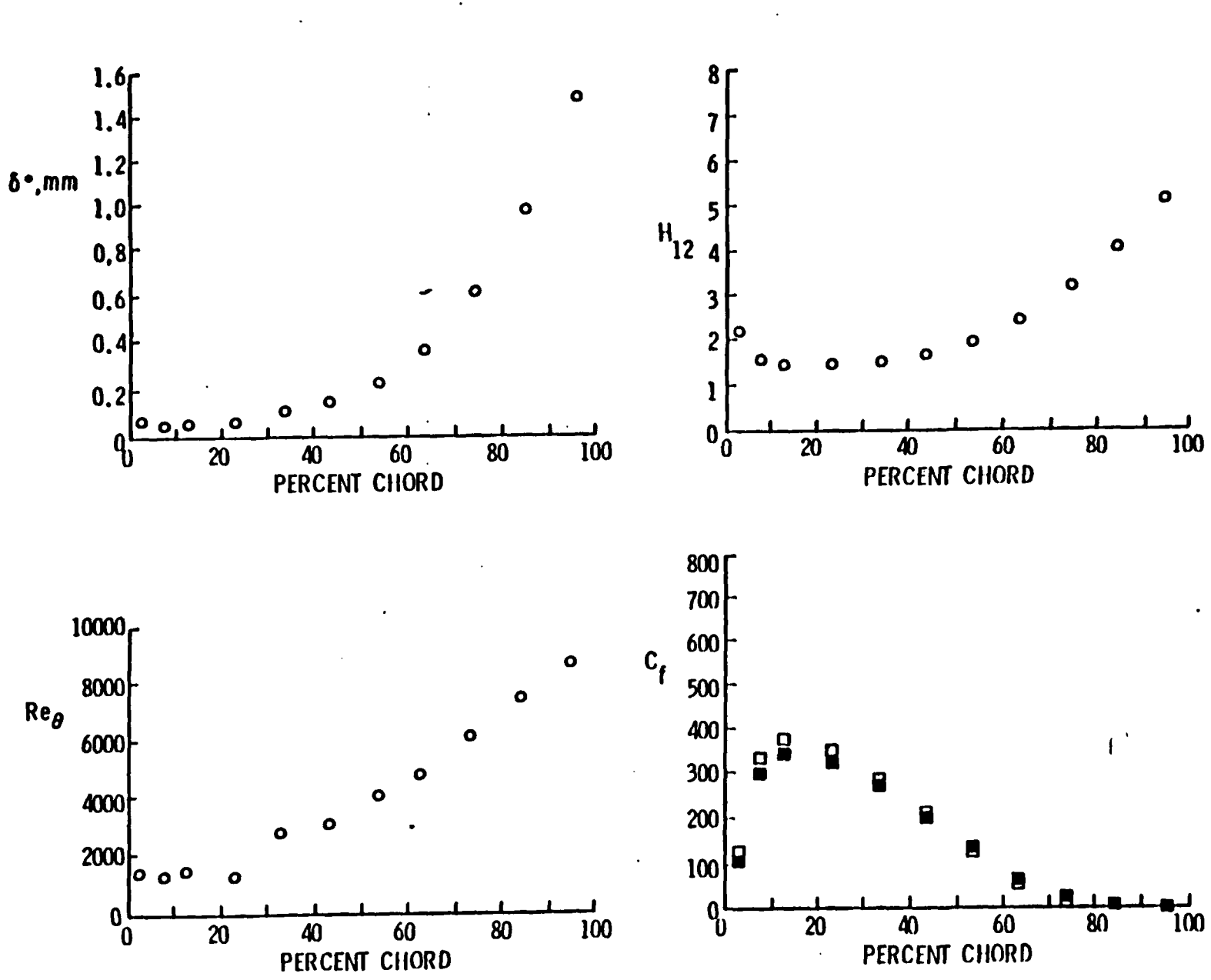

Figure 16. Variation of Displacement Thickness, First Shape Factor, Momentum Thickness Reynolds Number, and Skin Friction Coefficient on the Suction Surface (- Obtained From a Smoothed Cubic Spline Fit; - Obtained From a Least Squares Fit of the Wall-Wake Euqation; - Obtained from a Smoothed Cubic Spline Fit and the Ludweig-Tillman Equation)

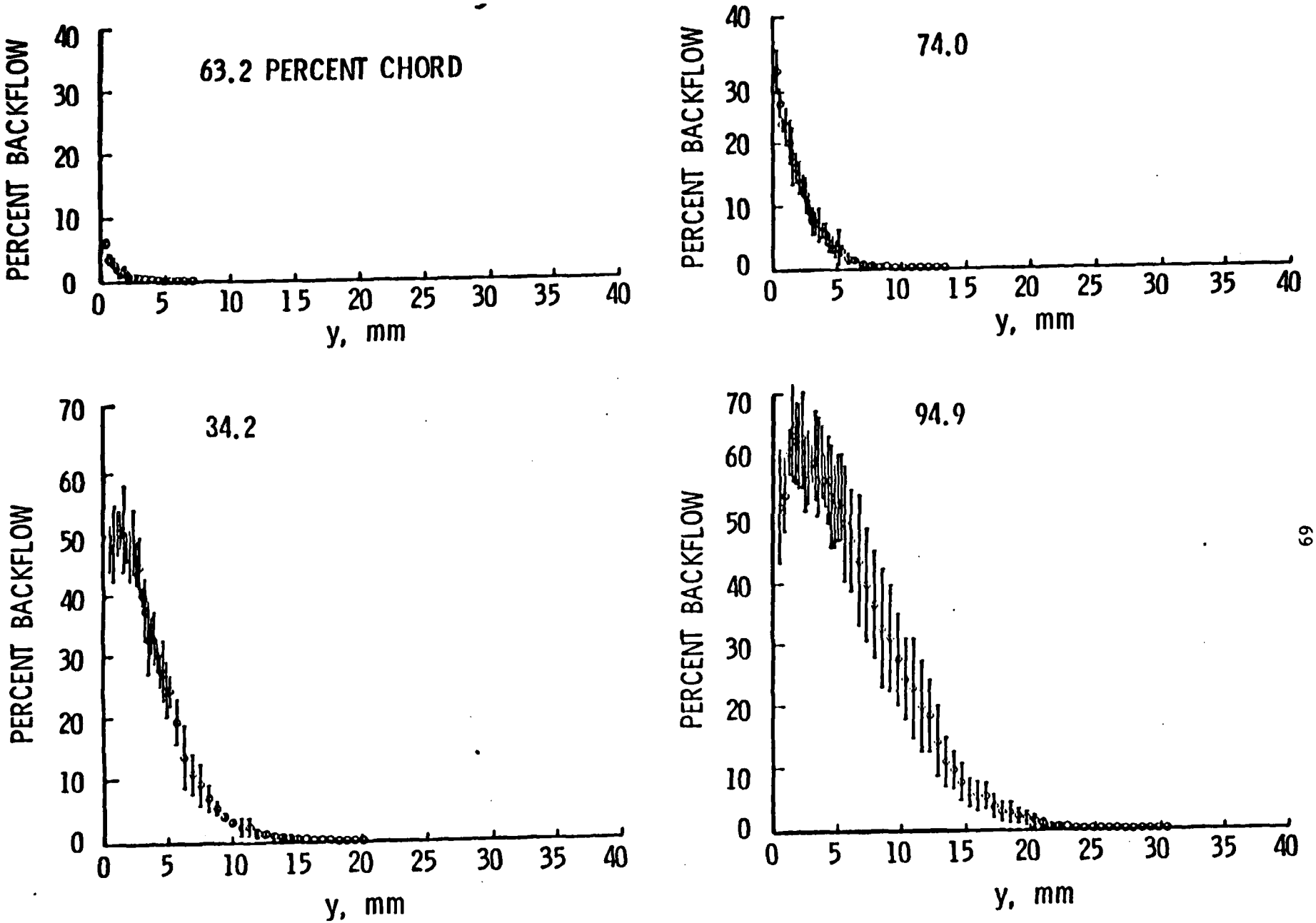

Figure 17. Instantaneous Backflow Measurements at the 63.2%, 74.0%, 84.2%, and 94.9% Chord Locations on the Suction Surface

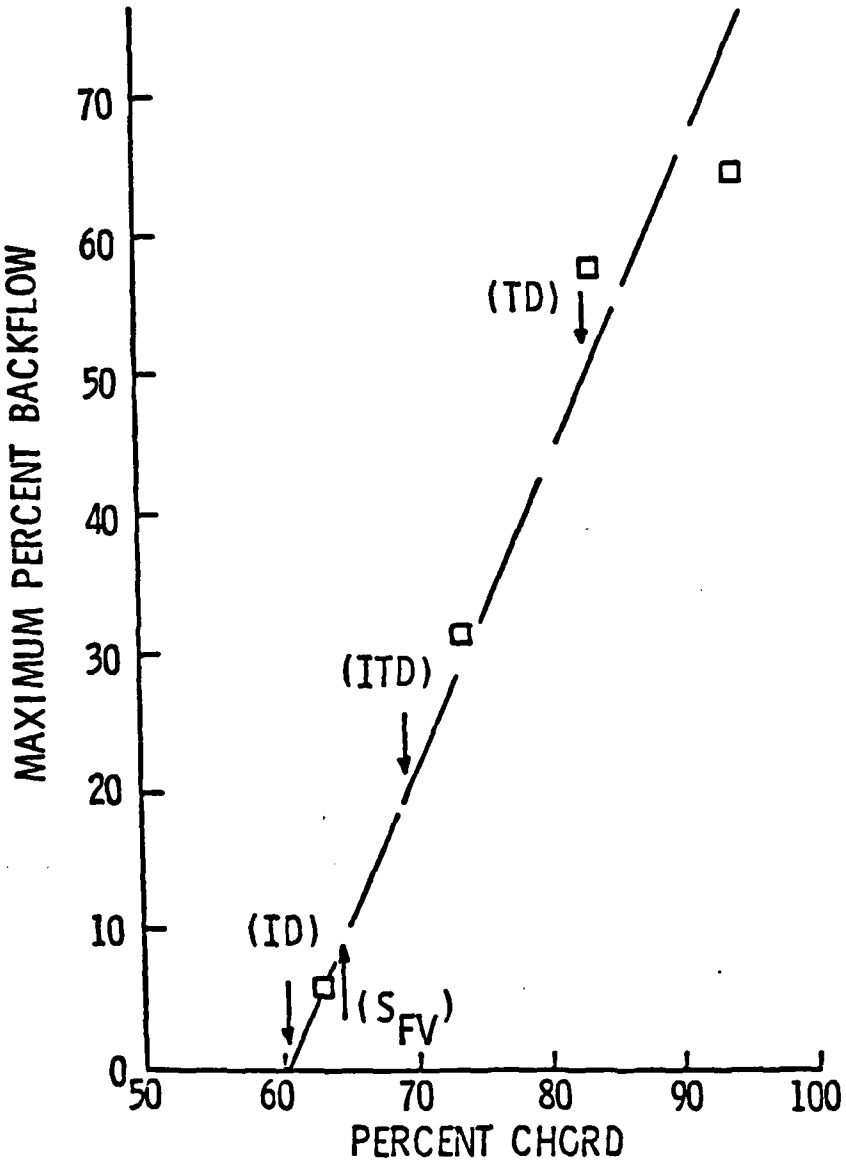

Figure 18. Maximum Percent Backflow on the Suction Surface (ID - Incipient Detachment; ITD - Intermittent Transitory Detachment; TD - Transitory Detachment; S_{FV} - Separation Point From Flow Visualization)

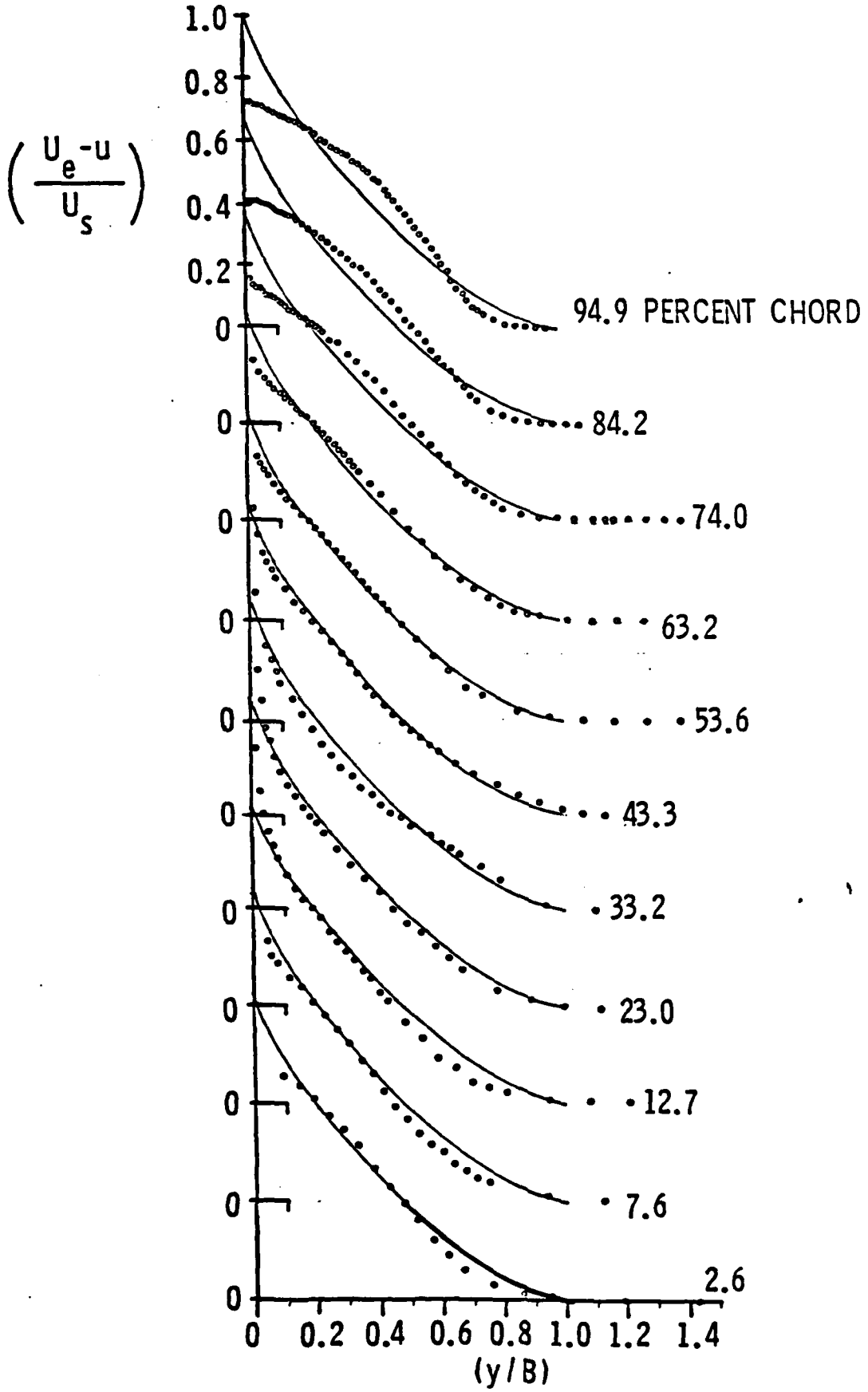

Figure 19. Reconstructed Suction Surface Boundary Layers in Defect Form With Perry-Schofield Similarity (Solid Lines)

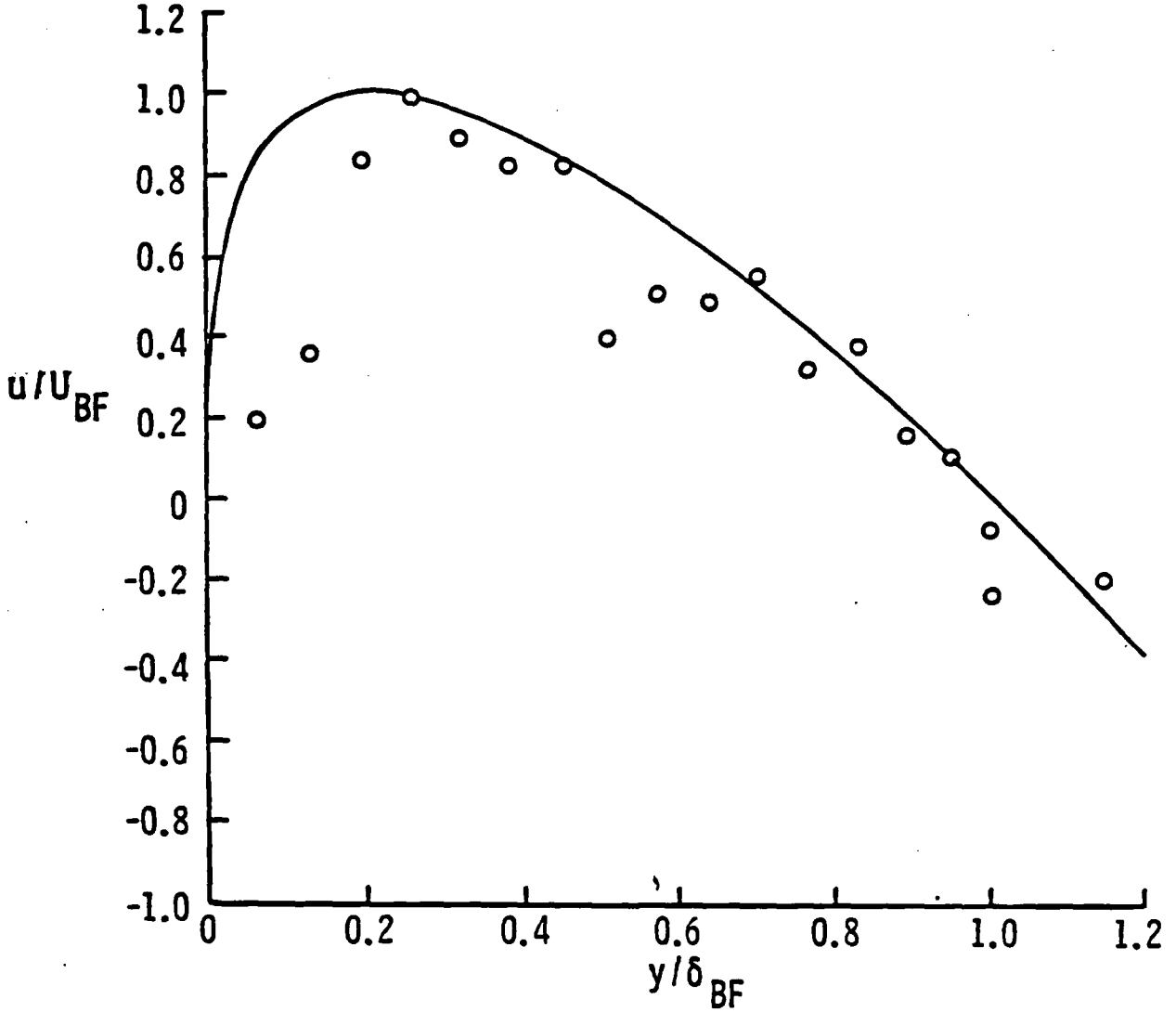

Figure 20. Backflow Similarity of the Reconstructed Boundary Layer at 94.9% Chord on the Suction Surface (The Solid Line Represents the Backflow Similarity of Data Measured by Simpson, Strickland, and Barr [1977] and Simpson, Chew and Shivaprasad [1981])

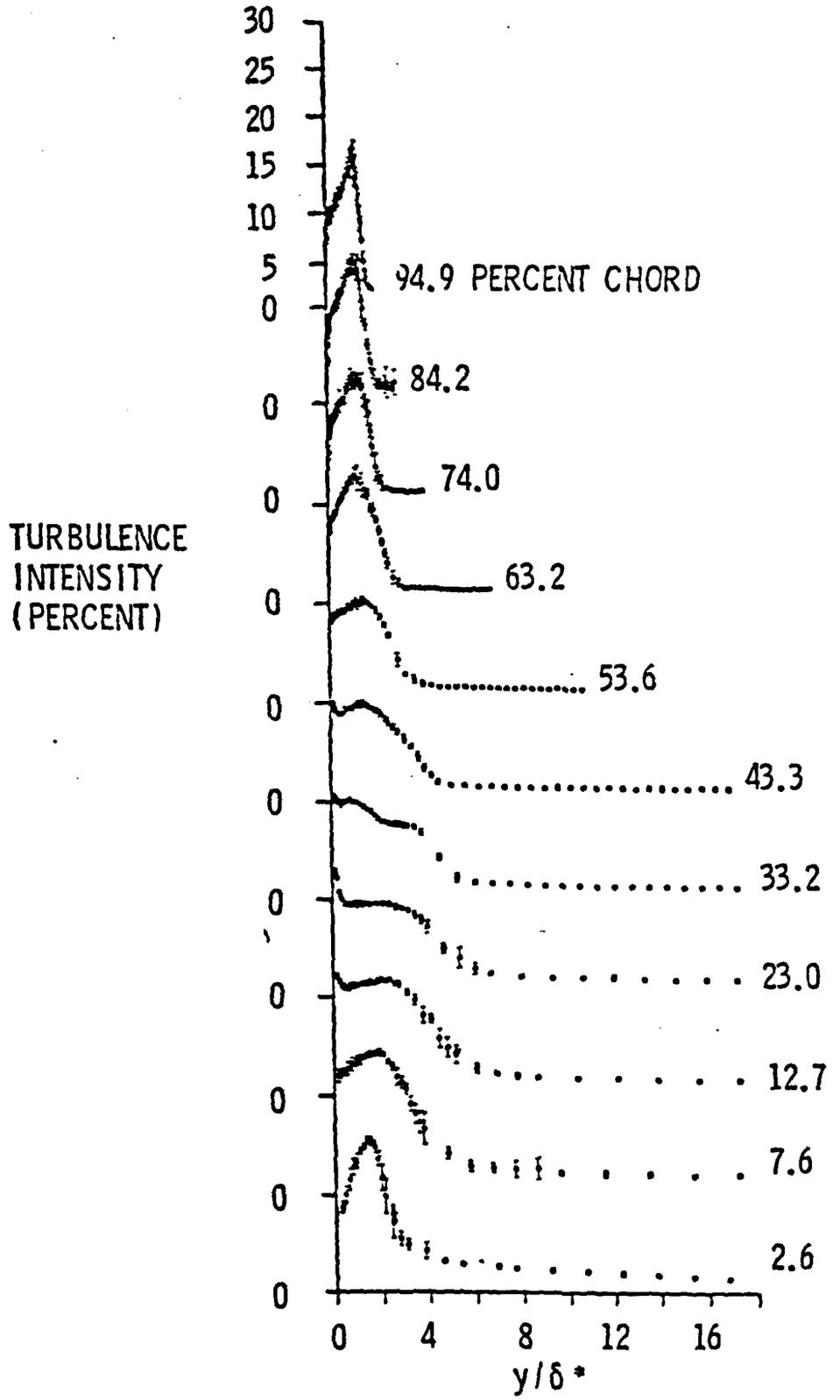

Figure 21. Turbulence Intensity Data for the Suction Surface Boundary Layers

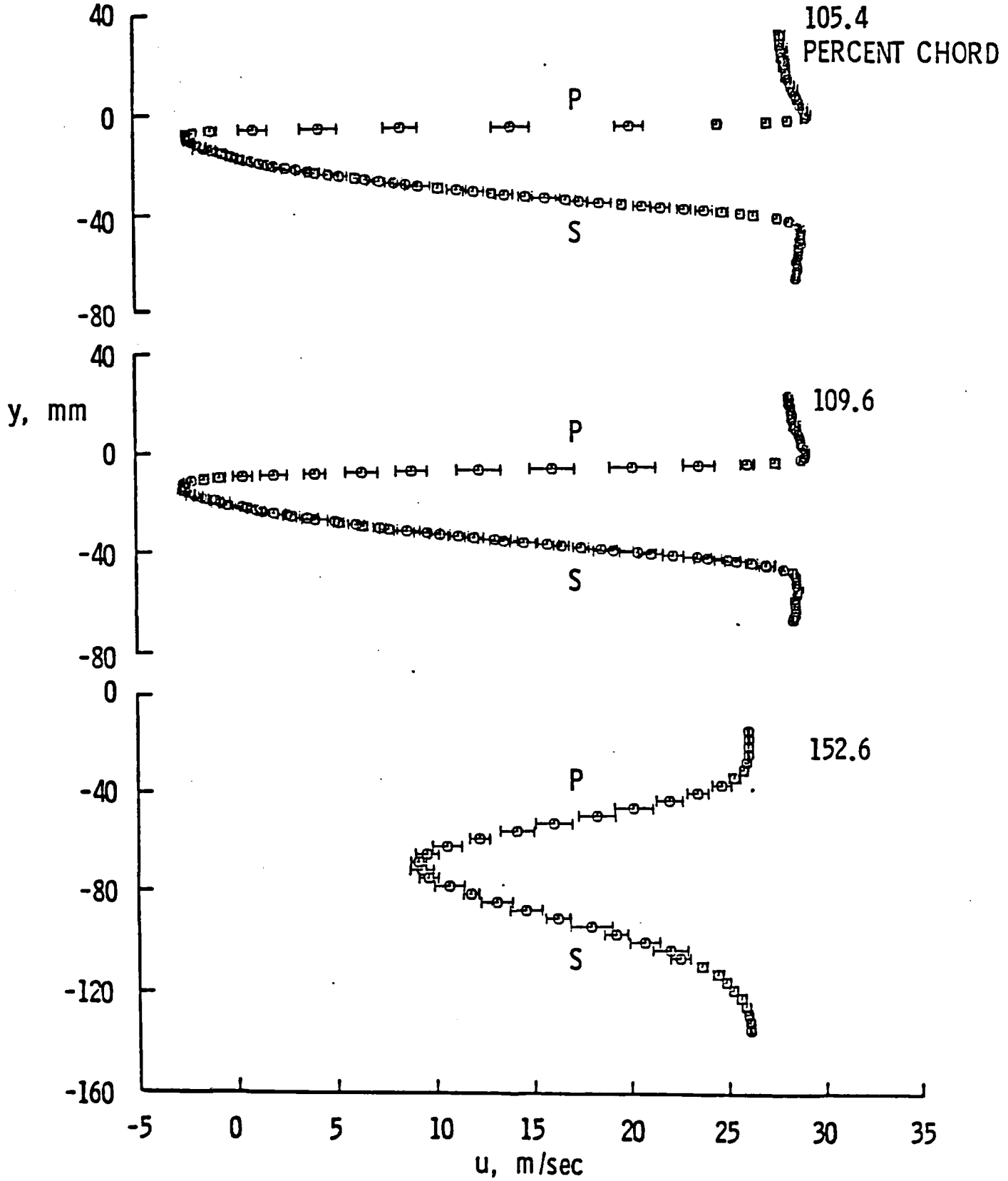

Figure 22. Measured Wakes (The Wakes at 105.4% and 109.6% Chord Were Measured With the LDV, While the Wake at 152.6% Chord was Measured With a Five-Hole Probe) (P - Pressure Surface; S - Suction Surface)

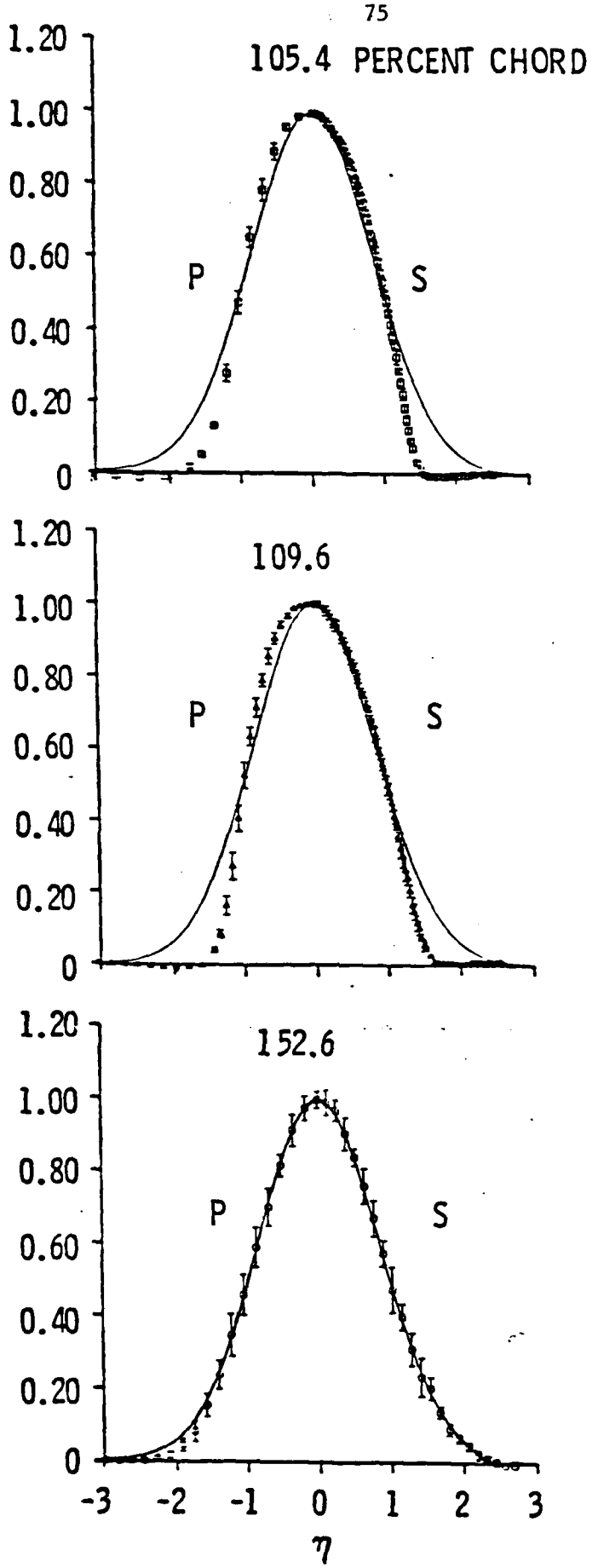

$$\frac{U_e - u}{U_e - u_{CL}}$$

Figure 23. Wakes in Defect Form With Gaussian Similarity (Solid Lines)
(P - Pressure Surface; S - Suction Surface)

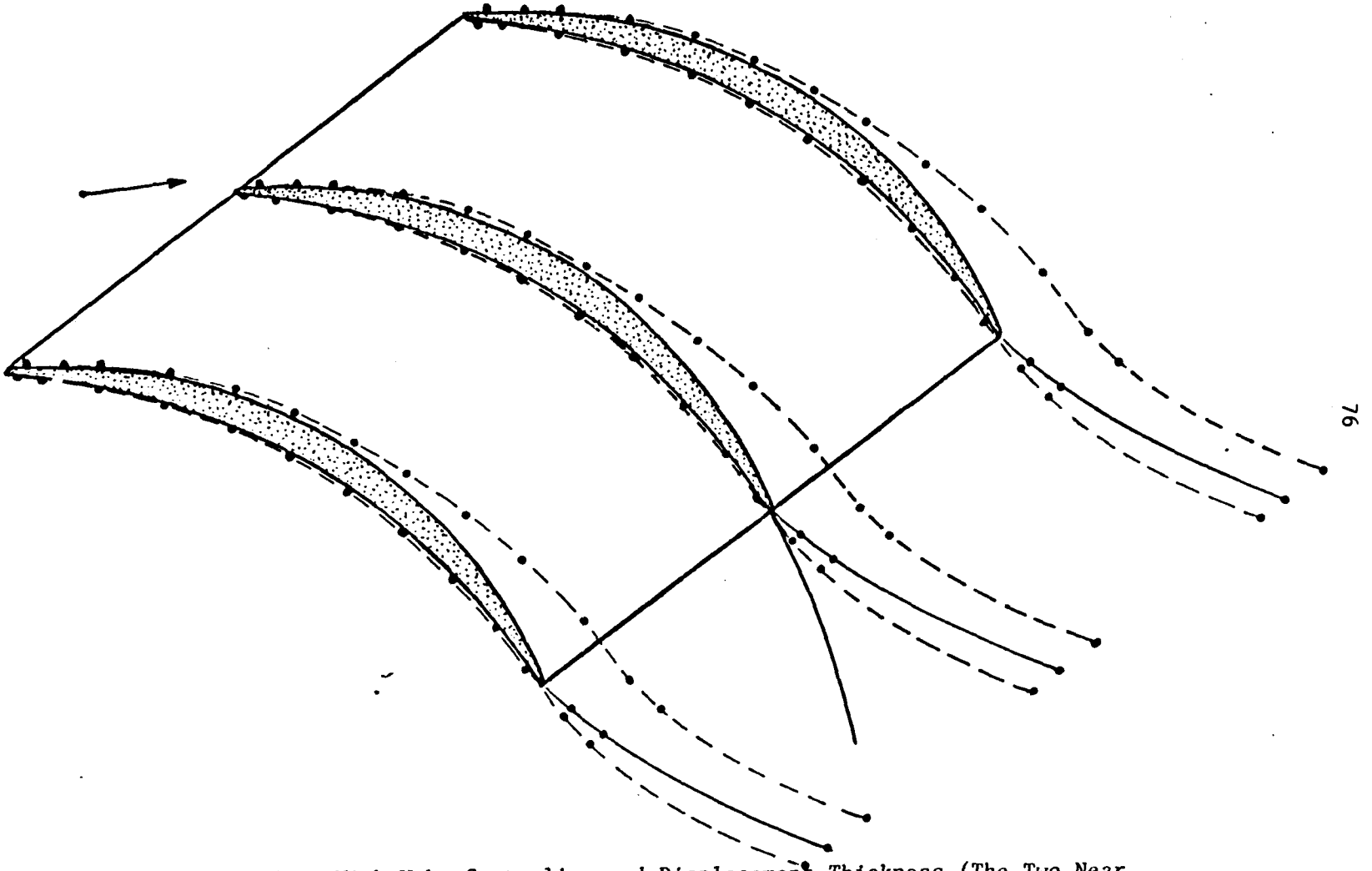

Figure 24. Cascade Blades With Wake Centerline and Displacement Thickness (The Two Near Wakes Were Measured With Respect to the Extended Pressure Surface Arc Which is Shown)

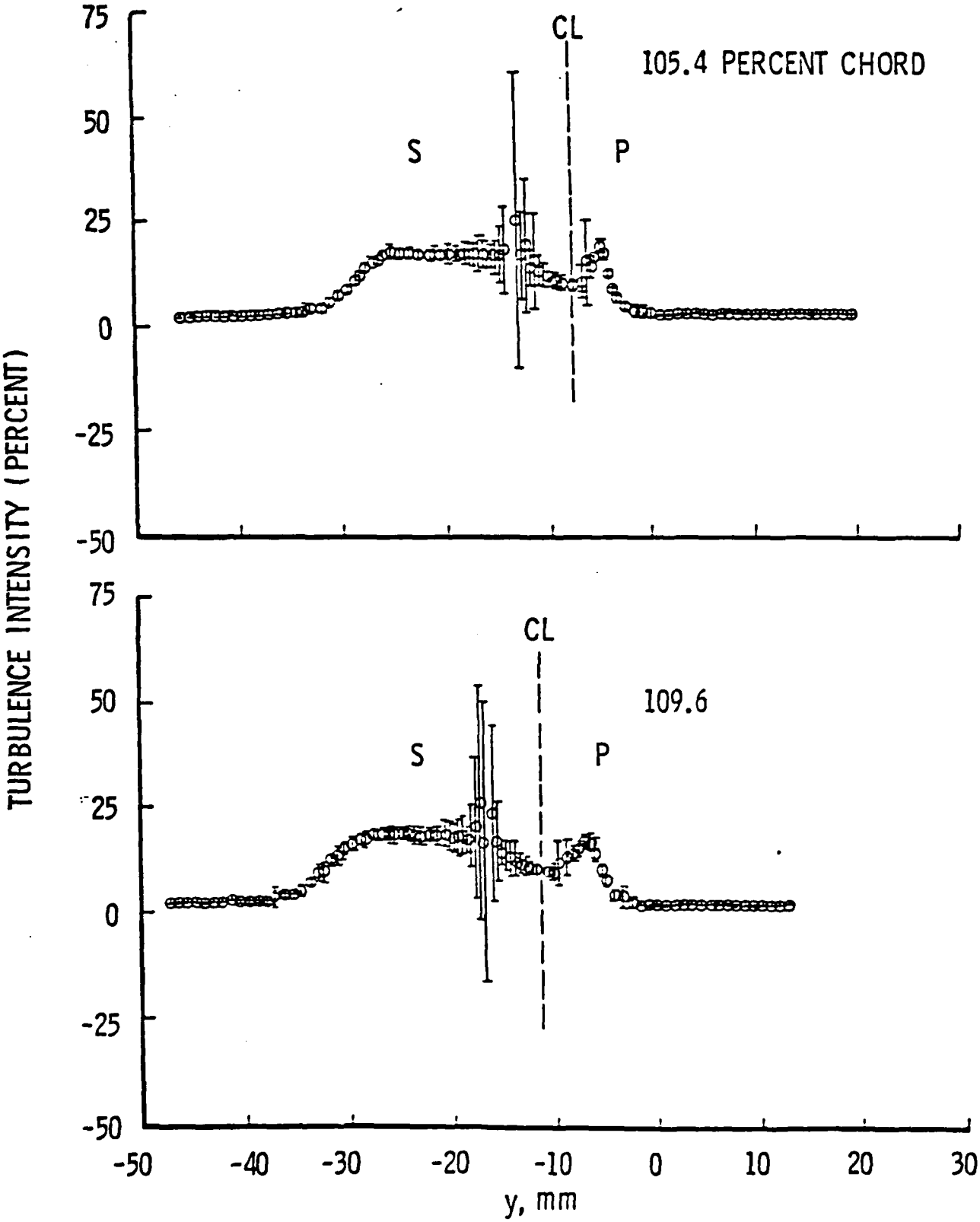

Figure 25. Turbulence Intensity Data for the Near Wakes (P - Pressure Surface; S - Suction Surface; CL - Wake Centerline)

END

10-86

DTIC